# Protein film electrochemistry

Butt, J.N.; Jeuken, L.J.C.; Zhang, H.; Burton, J.A.J.; Sutton-Cook, A.L.

# Protein film electrochemistry

Julea N. Butt[1†], Lars J. C. Jeuken[2†], Huijie Zhang[2], Joshua A. J. Burton[1], Alexander L. Sutton-Cook[1]

[1]School of Chemistry and School of Biological Sciences, University of East Anglia, Norwich Research Park, Norwich, NR4 7TJ, U.K.

[2]Leiden Institute of Chemistry, Leiden University, PO box 9502, Leiden 2300 RA, The Netherlands

[†]e-mail: j.butt@uea.ac.uk, l.j.c.jeuken@lic.leidenuniv.nl

**ABSTRACT:** Protein Film Electrochemistry (PFE) is a powerful suite of electroanalytical techniques used to investigate the properties of redox proteins. The proteins under investigation are adsorbed as a (sub-)monolayer film on an electrode surface. Direct electron transfer between the immobilized protein and working electrode gives rise to an electrical current that visualizes and quantifies redox processes occurring within the protein. Advantages of PFE include low sample requirements — typically less than a nanomole protein — high sensitivity and the ability to resolve redox chemistry in the electrochemical potential and time domains. This Primer provides a guide to using PFE for quantitative thermodynamic and kinetic descriptions of half-reactions (redox reactions) and coupled chemical processes, including ligand binding, ligand unbinding and redox catalysis. Applications of PFE in developing biosensors, facilitating energy conversion and resolving enzyme mechanisms are highlighted. Finally, the state-of-the-art and prospects for novel experimental and theoretical approaches are discussed.

## INTRODUCTION

Redox proteins are ubiquitous in biology. They perform electron transfer reactions and redox catalysis that are essential to life, for example, in photosynthesis and respiration. These functions are enabled by redox active cofactors, one or more per protein, including copper, molybdenum, heme, non-heme iron and flavin[1,2]. During physiologically relevant electron exchange the redox cofactors are positioned within 14 Å of one another[3]. Electron transfer between proteins is supported by cofactors near the protein surface. By contrast, redox catalysis may occur adjacent to cofactors buried deep within a peptide matrix. This allows redox transformation of the substrate in a site shielded from solvent, avoiding non-productive and possibly toxic redox reactions. Additional redox cofactors positioned as a chain enable electrons to be relayed between the active site and protein surface, **FIG. 1A**.

Protein film electrochemistry (PFE) — also termed protein film voltammetry (PFV) and protein monolayer electrochemistry — is a powerful tool for investigating the properties of redox proteins[4-11]. PFE studies protein electron transfer and redox catalysis using dynamic electrochemistry applied to a (sub-)monolayer film of redox active protein immobilised on the surface of a working electrode (WE). As shown schematically in **FIG. 1A**, there is direct electron exchange between the immobilised protein and WE, which gives rise to an electric current. The produced current visualises and quantifies redox processes within the protein. Using this approach, quantitative thermodynamic and kinetic descriptions of half-reactions (redox reactions) and coupled chemical processes, including redox catalysis, can be readily obtained. These descriptions result from considering direct electron transfer between the WE and adsorbed protein, **FIG. 1A**. PFE is different to experiments that use mediated electron transfer, where an additional redox-active species, often called a mediator, is introduced to shuttle electrons between the protein and WE.

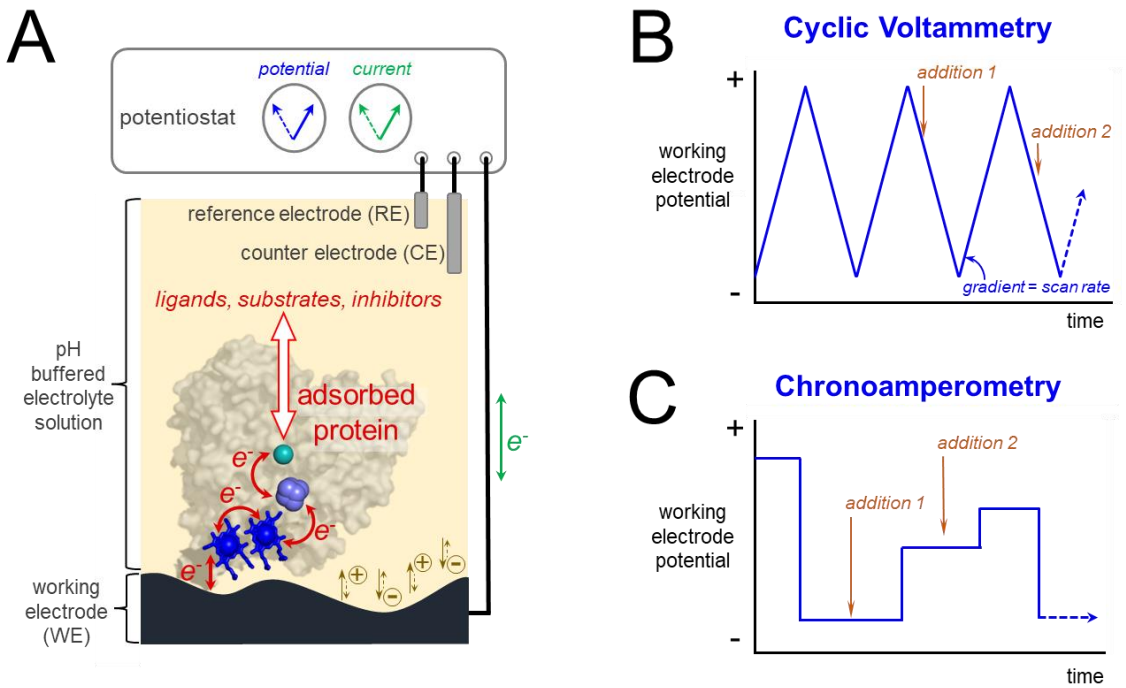


Fig. 1 | **Concept of protein film electrochemistry (PFE). A**| The protein of interest is adsorbed as a (sub-)monolayer film on a working electrode (WE). Direct electron transfer occurs between the WE and a redox cofactor terminating a chain of additional redox sites within the protein: heme (royal blue), iron-sulphur cluster (navy) and Mo (teal) cofactors (PDB ID: 1OGY). The protein retains full activity towards molecules and/or ions introduced to the surrounding electrolyte solution. The Mo cofactor is the active site of this redox enzyme. The hemes and iron-sulphur cluster relay electrons between the active site and the WE. A potentiostat applies defined and variable potential to the WE while simultaneously measuring the flow of current through that electrode. The measured current has two contributions: Faradaic current due to redox transformation in the protein (red arrows), capacitance due to migration of electrolyte ions (brown arrows). **B**| The excitation profile applied during cyclic voltammetry (CV) illustrating how scan rate is defined. **C**| An excitation profile for chronoamperometry (CA). Brown arrows indicate that reactants can be introduced at desired times in both CV (B) and CA (C).

PFE traces its roots back to the 1990s, when electrochemistry of adsorbed proteins was reported[12 13 14] that agreed with the properties defined by established biochemical assays of proteins in solution[6]. The adsorbed proteins retained functional integrity and the electrode-protein interactions could be considered to mimic those between the protein of interest and its biological redox partner. Today the advantages of PFE for revealing and understanding redox protein activity are widely recognised. The equipment is extremely low cost compared to modern biophysical methods and spectroscopies, with lower protein requirements, often sub-picomole in an adsorbed film prepared from a solution of less than a nanomole protein. The protein-coated electrode often survives changes in the solution to which it is immersed, meaning the impact of varying conditions can be readily assessed. Signals are sharp and high-resolution, enabling complex behaviour to be controlled, dissected, and elucidated because there are no contributions from relatively slow protein diffusion. In a single experiment, the current is measured across a wide, continuous potential range for the desired time — from under a second to several hours — allowing many different and defined changes to be made to the composition, pH and temperature of the immersion solution.

This Primer will describe the equipment typically used for PFE and provide the practical and theoretical background needed to perform and interpret electrochemical experiments. The article focuses on explaining how standard concepts available in electrochemistry[15,16] and biochemistry[17] textbooks

typically apply to PFE, illustrating how PFE describes redox couples, ligand binding and redox catalysis. Detailed discussions are kept to the simplest scenarios. However, more complex behaviours are touched upon, with references to works that illustrate how those results may be investigated and explained.

In this Primer, cyclic voltammetry (CV) and chronoamperometry (CA) will be focused on, as they are widely used and provide the most immediately intuitive and quantitative descriptions of protein redox chemistry. In CV, the WE potential is swept back and forth across a region of interest at a specified scan rate, **FIG. 1B**. The resulting current is measured simultaneously and reported as a cyclic voltammogram that plots current versus WE potential. In CA, the potential of the WE is stepped instantaneously between defined values at specified time points, **FIG. 1C**. The resulting current is reported versus time in an 3mperomograms. Conditions can be changed as desired, for instance, a reactant can be introduced in both types of experiment.

It is important to recognise that the current in both CV and CA has two components that are superimposed[15]. The Faradaic current is due to electron transfer between the electrode and redox active proteins in the (sub-)monolayer film, **FIG. 1A** (red arrows). Non-Faradaic current (capacitance) is due to charging and discharging of the electrode–solution interface and electrons are not transferred across that interface, **FIG. 1A** (brown arrows). PFE is interested in the Faradaic current, as it reports the redox chemistry of the protein. Care must be taken to accurately extract the Faradaic current from the measured current. By convention, Faradaic current is negative during net reduction and positive for net oxidation.

## EXPERIMENTATION

The equipment needed for PFE depends on the desired application, but requires at least a potentiostat[18], an electrochemical cell and analytical software. The electrochemical cell contains a counter electrode (CE) and reference electrode (RE) in addition to the WE. During measurements the WE may be stationary or rotating. The latter is particularly useful when studying redox catalysis and a rotating disk electrode (RDE)[15] allows controlled substrate delivery to the adsorbed enzyme. These experiments can be extended to use a rotating ring disk electrode (RRDE)[15], which forces the products of enzyme catalysis to flow across a second WE — a concentric ring around the central enzyme coated disk electrode — for analysis by amperometry.

### *Potentiostats and working electrode rotators*

Potentiostats can be purchased from many manufacturers. Alternatively, the instrument can be made in-house[19] for a fraction of the cost. The ideal instrument will depend on the specific requirements and funds available. All potentiostats can perform basic CV and CA methods. The specifications that require special attention for PFE are current range; scan rate or band width range; capacity for $iR$ compensation, where $I$ is current and $R$ is resistance; ability to use RRDEs; and ability to perform analogue CV by applying a true linear voltage ramp to the WE, **FIG. 1B**, in addition to CV, which approximates the linear ramp with a staircase waveform, and is the primary CV method in contemporary potentiostats[18].

PFE typically uses WEs with a surface area of < 1 $cm^2$, scan rates in CV < 100 V/s and potential steps in CA of < 1 V. Under these conditions, currents are in the nA to mA range, which is adequately covered by all commercial potentiostats. However, if the intended applications are in bioelectrocatalysis with WEs that have larger surface areas, higher current ranges might be required.

When studying the kinetics of electron transfer or coupled reactions, fast-scan CV (scan rate >100 mV/s) is a powerful tool[6,20-22]. As a result, the scan rate capabilities of the potentiostat should be considered. The area under a redox peak, the non-catalytic CV, can deviate from theory when using staircase CV[23], which is the standard method in most contemporary potentiostats[18]. If the protein coverage analysis needs to be accurate or when studying reaction kinetics, potentiostats that can measure analog CV should be considered.

For both non-catalytic fast scan and catalytic PFE, currents in the high μA to mA range can be obtained. This can lead to significant potential drops due to solution resistance[24]. As current flows through the electrochemical cell, a potential difference is required across the electrolyte solution to drive ion mobility and overcome solution resistance. As a result, the potential at the WE interface has a lower magnitude than the potential applied by the potentiostat. For instance, if the solution resistance is 100 Ω, a current of 100 μA leads to a potential shift of 10 mV ($V = iR$, where $V$ is potential). Potential drop can be reduced by minimizing the solution resistance, but can also be compensated for by potentiostats with $iR$ compensation capabilities[24].

The sensitivity of potentiostats to electronic noise[18] is an important property. However, this property cannot be determined from specifications and can only be established by trying different potentiostats under laboratory conditions. Where possible, the electrochemical cell should be placed in a Faraday cage to reduce electronic noise. Suitable Faraday cages are readily constructed from commercially sourced electrical boxes, typically steel, with holes for the electrical leads. Alternatively, Faraday cages can be made from a wire mesh, which enables the electrochemical cell to be observed during measurements, plus easy access for electrical leads and other connections, such as gas lines.

Rotators for use with RDEs are available from several suppliers. Differences include the ability to use RRDEs, an integrated enclosure for the rotator shaft, variable distances between the controller and rotator shaft, and the range of electrodes and electrochemical cells compatible with the rotator. The choice of instrument will be influenced by the ring and disk electrode materials, and whether the electrochemical cell needs to be serviced by gas supply lines or temperature-controlled water. Anaerobic experiments also need to consider how readily the rotator can be positioned and operated within a nitrogen-filled chamber.

***Electrochemical cells, CE and RE***

There are many manufacturers of electrochemical cells, cEs and rEs. For many PFE applications, a tailor-made electrochemical cell is worth considering, but requires access to a glass blower or fine-mechanical facility. The wide range of PFE applications means there is no single best cell design. Variables to consider include the distance between the RE and WE, the need for a RDE or RRDE, and auxiliary methods, such as illumination for photo-electrochemistry[25,26] or combination with microscopy or spectroscopy[27]. In **FIG. 2**, several example cell designs are provided with a short explanation of their properties and specific applications.

Alongside the cell, the three electrodes — or four electrodes for a RRDE — are key to PFE. The CE ensures electroneutrality of the electrolyte solution. For every Faradaic electron transfer at the WE, an opposite electron transfer is required at the CE. In PFE, the CE is almost always platinum. Electrochemical currents in PFE are typically low mA or less, meaning a small platinum wire (< 2 cm) is sufficient. The most used and convenient RE is Ag/AgCl (saturated KCl) although others can be used. Trace amounts of chloride ions, which leak out of the RE into the electrolyte, can affect the results for some applications. In this case, a double junction RE is advised, where the Ag/AgCl RE is placed inside a jacket. This can be achieved by sourcing a double-junction RE or by designing an electrochemical cell

with a double junction, **FIG. 2B,C**. Drift from the quoted potential[15] can occur if the RE is not maintained. rEs are easily calibrated by comparing the open cell potential with respect to a trusted RE. If a trusted RE is not available, the CV of a redox couple with known reduction potential — such as ferri/ferrocyanide — can be measured under controlled temperature, pH and ionic strength. Potentials measured versus a Ag/AgCl (saturated KCl) RE at 25°C are typically converted to values versus the standard hydrogen electrode (SHE) by adding +0.197 V[15].

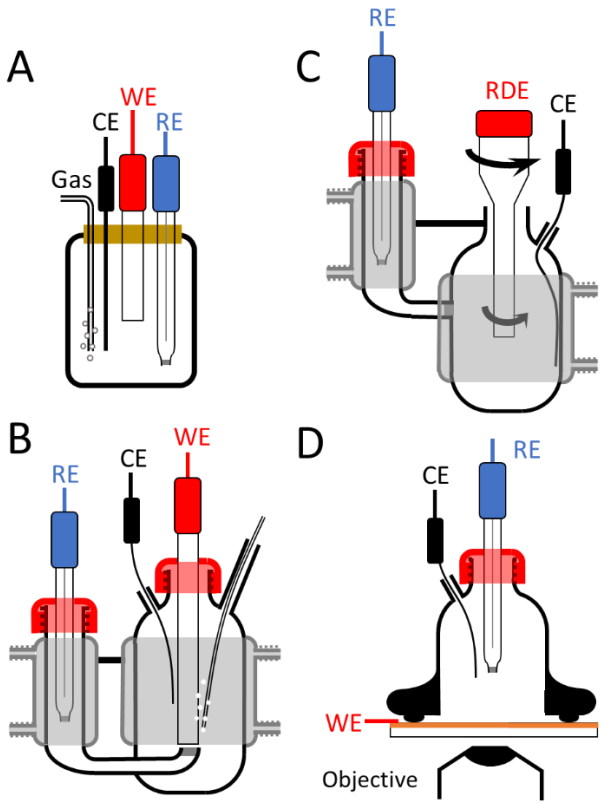


Fig. 2 | **Schematics of electrochemical cells. (WE = working electrode; CE = counter electrode; RE = reference electrode). A** | A basic electrochemical cell such as can be purchased commercially for use with a rod-shaped WE. **B** | An optimised electrochemical cell for stationary electrochemistry with a rod-shaped WE. The main cell has a water jacket (grey) for temperature control. The RE is placed to the side of the main cell to enable separate temperature control. Leakage of RE solution (for instance saturated KCl solution) into the main cell is minimised by using a second junction (either a glass frit or a luggin capillary). The second junction is placed close to the WE to minimize solution resistance ($R$) and hence potential drop ($iR$ drop). **C** | Cell for use with a rotating disk electrode (RDE). The WE is a disk on the lower face of the rotated housing. The cell volume should be sufficiently large to preclude a significant drop of substrate concentration during measurement of redox catalysis. The CE and luggin tip are positioned to minimise turbulence. **D** | A basic electrochemical cell for working with a plate-shaped WE. If a transparent gold electrode is used — for example a <50 nm thick gold film on a glass slide — this cell can be combined with epi-fluorescent microscopy in an inverted microscope. Here, the glass cell is placed on top of the WE with an O-ring, which is not air-tight, and oxygen can slowly diffuse to the plate electrode from the side.

### *Working electrodes*

In PFE, the most important electrode is the WE. To form an electroactive protein film, the redox protein needs to be immobilised on the WE while retaining its native tertiary and quaternary structure and activity. Proteins can be physisorbed or chemisorbed on the electrode surface, with physisorption being the most common[28]. Many proteins are adsorbed via electrostatic interactions, although rarer hydrophobic interactions are known. Electrostatic interaction and protein immobilisation are affected by the ionic strength and pH of the electrolyte, as the pH determines the charge on the protein surface. Electrolyte solutions in PFE are always pH buffered. To control the potential drop across the WE without disrupting the electrostatic interaction between the protein and WE, an ionic strength of ~0.1 M is often a good compromise. Adsorption/desorption is an entropic process, making temperature an

important variable. Lower temperatures improve the film stability but lower catalytic rates. Chemisorption can be achieved by reacting an amino acid side chain group with the electrode surface[29] or by affinity interaction[30]. Chemisorbing proteins is more time-consuming than physisorption but can lead to more stable protein films[31].

Electron transfer rates decrease exponentially with distance between the donor and acceptor. Suitable electron transfer kinetics (< ms) for PFE requires the distance between at least one redox cofactor and the electrode surface to be less than 2 nm. In practice this means that the protein needs to orient correctly upon adsorption, **FIG. 1A**. One approach is to use a heterogeneous electrode surface, in terms of both geometric structure and surface chemistry. Heterogeneity increases the possibility that some immobilised proteins are correctly orientated, even if most are electrochemically silent.

Three widely used WE materials are pyrolytic graphite edge (PGE) plane, modified gold and indium-tin oxide (ITO), although others have successfully been used. The surface of PGE electrodes exposes the side edges of the graphene sheets, enabling the carbon interface to form a rough surface with multiple carbon oxide chemistries. PGE electrodes are quickly and easily cleaned by polishing the surface with an aqueous slurry of alumina or diamond powder, typically 1-micron particles, followed by a brief treatment in a water-bath sonicator to remove particles. This quick preparation means PGE electrodes are a convenient experimental tool. The PGE surface is negatively charged due to presence of carboxylic acids. Consequently, co-adsorbates are required for redox proteins that are negatively charged or have a negative surface charge close the co-factor orientated towards the electrode surface. Good co-adsorbates are polylysine, neomycin or polymyxin B, which are added to the electrolyte or protein solution before they are applied to the electrode. The surface of PGE and other graphite electrodes can also be controlled by adsorption of polycyclic aromatic hydrocarbon derivatives, such as pyrene derivatives, which form stable pi-stacking interactions[32]. Alternatively, PGE can be chemically modified to alter its surface chemistry by electrografting. For instance, reduction of aryl diazonium salts forms radical anions that covalently bind with the carbon surface[33].

Barring some exceptions, bare gold is not a suitable electrode for PFE. However, gold electrodes have surface chemistry that can be controlled by forming self-assembled monolayers (SAMs) of thiol-derivatives, where the thiols form a stable gold-thiol bond[34-37]. This enables careful optimisation of the electrode surface chemistry by forming reproducible hydrophilic/hydrophobic surfaces with negative and/or positive groups. Gold electrodes can be crystalline, ultrasmooth, rough or prepared from nanoparticles. The exact geometry of the gold electrode affects the structure of the SAM[34], which affects the protein film formation and PFE results. PFE is typically performed with freshly prepared SAMs. A drawback of using modified gold electrodes is that SAMs are typically formed over many hours, limiting the number of experiments that can be performed in a day.

ITO electrodes are increasingly being used. They are optically transparent, enabling simultaneous absorbance spectroscopy or photobioelectrochemistry. To increase the electrode area and roughness, ITO nanoparticles can be used to create mesoporous surfaces with greater opportunity for protein adsorption[38-40]. Preparation methods include using polystyrene beads as a template, around which the ITO nanoparticles are deposited. This results in more highly ordered[38,41], honeycomb-like electrode materials than direct electrophoretic deposition[40].

***Film preparation***

The protein film is typically prepared by briefly incubating the freshly polished or prepared WE surface in a small volume of protein solution, just enough to wet the surface, typically μM concentration.

Longer incubation times may be used with more dilute protein solutions. Loosely bound material may be removed from the WE surface by rinsing with an appropriate pH buffered-electrolyte solution before the electrode is introduced to the electrochemical cell. It is advised that the film forming solution not be allowed to dry on the WE. If the solution does dry on the WE, it can result in behaviour that is difficult to reconcile with established biochemical assays, presumably due to partial or complete loss of protein structure on adsorption.

***Anaerobicity and temperature***

For experiments with applied WE potentials of approximately -0.1 V vs SHE and lower, oxygen needs to be removed from the electrolyte, unless the aim is to measure oxygen interaction with the protein film. For stationary electrodes, purging the electrolyte with nitrogen or argon gas is typically sufficient. For lengthy experiments (> hours), gas that has been humidified by bubbling through water can be used to reduce solution evaporation, which would change the ionic strength or pH of the electrolyte. When using a RDE, anaerobicity can be achieved with closed electrochemical cells, as the rotating electrode stirs the electrolyte, rapidly drawing in air or gas. Closed RDE systems can be challenging to design. Open systems may be preferred and are most readily used within a glove box — a $N_2$-filled chamber — to ensure anaerobic conditions.

Temperature is an important parameter because it is a primary determinant of reaction rate. Temperature is most conveniently controlled by placing the electrochemical cell in a temperature-controlled solution. Commercial or tailor-made electrochemical cells can be designed with an external water jacket, where the temperature is set with a circulating water bath. However, the potential of the RE is temperature dependent. For accurate control of the applied potential, the RE can be placed in a side-arm of the cell with its own temperature-controlled water jacket, **FIG. 2B,C**.

***Software***

All commercial potentiostats come with software to control the hardware. This software is often able to perform a basic analysis of voltammograms and amperomograms, but capabilities are very limited. A versatile, freely available software is QSoas[42-44]. QSoas enables basic data analysis, such as smoothing and baseline subtraction capabilities to remove non-Faradaic currents. QSoas also allows non-linear curve fitting, creating a flexible fitting platform to analyse catalytic waves with complex kinetic models. QSoas is still being expanded, with recent additions including calculation of redox peaks at increasing scan rate.

Electronic noise can often be eliminated by careful design and maintenance of the electrochemical equipment and its location[18]. If noise persists, its contribution to the measured data can be lowered in several ways[18]. Random noise can be removed by signal averaging applied to consecutive steady-state measurements. Regular, periodic noise can be removed by fast Fourier transform techniques, which are included in the controlling software or QSoas. If such methods are used, it is important to inspect the data carefully to ensure that key information hasn't been distorted.

***Further considerations***

The experimental and equipment requirements outlined above are for basic PFE experiments. However, there are many insightful and exciting examples where PFE is expanded beyond the basic setup. These may require adjustments to the electrochemical cell and electrodes or additional equipment. Examples include the use of microelectrodes[45,46], combining PFE with spectroscopy[27,47-52], using high or low (< 0 °C) temperatures[53] or specialised gas mixtures. A full discussion is beyond the scope of this Primer, but three options could be considered when purchasing a potentiostat. All

potentiostats perform basic CV and CA, but more advanced methods, such as electrochemical impedance spectroscopy, are not standard. Impedance spectroscopy can be useful when studying SAM formation on gold WEs. When studying catalysis, a RRDE can be useful[54], but requires a potentiostat with the ability to measure two or double WEs. Finally, when using microelectrodes, the ability to accurately measure pA and sometimes fA currents is necessary.

## RESULTS

A few scenarios can provide the basis to describe many redox-active proteins.. This section details the corresponding Faradaic currents and the information that can be extracted. Because the experimentally measured currents include both Faradaic and non-Faradaic contributions, it is important to reiterate that the latter must be subtracted from the measured currents prior to analysis, **FIG. 3A,B**. This subtraction may make use of baseline currents measured in an identical experiment without adsorbed protein[55]. Alternatively, the non-Faradaic currents may be modelled using QSoas[42-44]. Good practice is to always measure the baseline response. This measurement enables informed modelling of the charging currents and minimises the likelihood that Faradaic currents from contaminants or additives reacting directly at the electrode will be mistaken as from the protein of interest [8,55-57].

### *Mapping out half-reactions*

Reversible oxidation and reduction of an adsorbed protein by varying the WE potential can be described by a half-reaction: Ox + $ne^-$ → Red. When this process is uncomplicated by slow interfacial electron transfer kinetics or coupling with a chemical reaction, cyclic voltammetry reveals peaks that are superposed on the non-Faradaic baseline response. These peaks are mirror images along the potential axis, **FIG. 3A,B.** Peaks detected when sweeping to increasingly positive WE potentials correspond to protein oxidation and have positive currents. Peaks with negative currents that are measured by sweeping to increasingly negative WE potentials describe cofactor reduction. Such peaks are sometimes termed non-catalytic because they do not arise from redox catalysis. When interpreting each non-catalytic peak, the current magnitude, $|i|$, can be described by [15,58]:

*Equation (1)*

$$|i| = \frac{exp\left(\frac{nF}{RT}(E - E^0)\right)}{\left(1 + exp\left(\frac{nF}{RT}(E - E^0)\right)\right)^2} \cdot \frac{n^2F^2vA\Gamma}{RT}$$

where $E$ is the WE potential, $E^o$ the reduction potential and $n$ the number of electrons transferred in the corresponding half-reaction, $F$ = Faraday's constant, $R$ = gas constant, $T$ = absolute temperature, $v$ = voltametric scan rate (V/s), $A$ = WE surface area (cm$^2$), and $\Gamma$ = electroactive redox protein coverage (moles/cm$^2$). The peak currents ($i_p^{ox}$ and $i_p^{red}$ , **FIG. 3A**) have equal magnitude. The potentials of maximum current ($E_p^{ox}$ and $E_p^{red}$) are those of $E^o$. The stoichiometry of electrons transferred in the half-reaction is defined by the half-height peak width ($W_{1/2}$) using Equation (2).

286 *Equation (2)*

287 $$W_{1/2} = \frac{2RT}{nF}\ln\left(3 + 2\sqrt{2}\right)$$

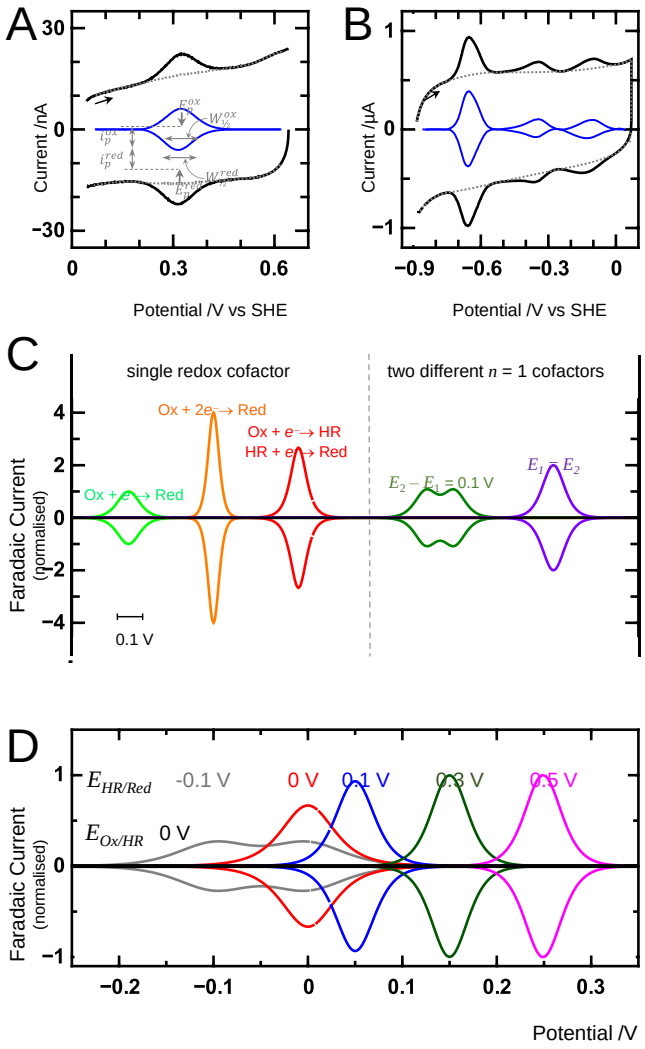


Fig. 3| **Non-catalytic peaks in the cyclic voltammetry (CV) of adsorbed proteins. A**| Cyclic voltammogram (black) of a protein with a single $n$ = 1 cofactor. Scan rate 10 mV $s^{-1}$, black arrow shows the scan direction. Currents due to capacitance (grey dotted line) and Faradaic currents (blue) are also shown. Peak potentials ($E_p$), peak currents ($i_p$)and half-height widths ($W_{½}$) are indicated for the oxidation (ox) and reduction (red) peaks. The peaks originate from a $Cu^{2+/+}$ cofactor. **B**| Cyclic voltammogram (black) of a protein with a single $n$ = 2 couple and two $n$ = 1 cofactors. Scan rate 19 mV $s^{-1}$, black arrow indicates the scan direction. Charging currents (grey dotted line) and Faradaic currents (blue) are also shown. The peaks originate from $[3Fe\text{-}4S]^{1+/0}$, $[4Fe\text{-}4S]^{2+/1+}$ and $[3Fe\text{-}4S]^{0/2-}$ cofactors in order of increasingly negative reduction potential. **C**| Examples of the Faradaic currents typically produced by protein cofactors. For a single cofactor moving between oxidised (Ox) and reduced (Red) states with $n$ = 1 (light green) and $n$ = 2 (orange). For a single cofactor where two sequential $n$ =1 processes convert Ox to Red via a half-reduced (HR) state (red) and the reduction potentials for the two half-reactions are equal. For two cofactors moving between their Ox and Red states in $n$ = 1 processes with $E_2 - E_1$ = 0.1 V (dark green) and $E_1 = E_2$ (purple). **D**| Faradaic currents that can be produced by a single cofactor having two sequential $n$ = 1 process where conversion of Ox to Red via a half-reduced (HR) state is described by $E_{Ox/HR}$ = 0 V and the value for $E_{HR/Red}$ is as indicated. In practice, measured non-catalytic peaks, for example panels A and B are typically broader and less symmetrical about the potential axis than theory predicts.

At 25°C, $W_{1/2}$ = 90 mV for $n$ = 1, **FIG. 3C** green, and $W_{1/2}$ = 45 mV for $n$ = 2, **FIG. 3C** orange. However, pure $n$ = 2 reactions are rarely observed in proteins. More often cofactors — such as flavin, molybdenum and tungsten — are described by two consecutive $n$ = 1 half-reactions that link the oxidised, half-reduced and fully reduced levels. For this scenario, equations relating the peak shape and $W_{1/2}$ to the separation of reduction potentials have been presented[59]. **FIG. 3D** illustrates how the form of the non-catalytic peaks is defined by the relative reduction potential values for the consecutive half-reactions in REF[59] (page 147) . In practice, small deviations from the ideal descriptions are often seen. For example, $E_p^{ox}$ and $E_p^{red}$ may differ slightly such that $E^o$ is reported as the average of the measured values.

Because the protein film is comprised of a finite number of molecules and cofactors, the Faradaic current drops to zero when a redox reaction is complete, **FIG. 3**. The peak area defines the moles of electroactive redox cofactor ($A.\Gamma$) in the protein film through Equation (3)

*Equation (3)*

$$A.\Gamma = \frac{\Pi}{nFv}$$

where $\Pi$, the voltammetric peak area, has units of Amps.Volts (= Coulombs.Volts/sec). The areas of the oxidation and reduction peaks will be equal for a fully reversible redox process.

For proteins with more than one half-reaction, each reaction contributes Faradaic currents and the responses are additive[12,48,60-64]. For the example presented in **FIG. 3B[12]**, the widely spaced peaks immediately reveal three half-reactions. A cooperative $n$ = 2 process appears as a prominent and narrow pair of peaks at more negative WE potentials, compared to an equivalent number of $n$ = 1 centres at more positive WE potentials. This distinction arises because the current magnitude varies as $n^2$ (Equation 1); $W_{1/2}$ varies as 90/$n$ (Equation 2); and the peak area as $\Pi$ (Equation 3). Multiple half-reactions are readily detected when $E^o$ values are separated by > 0.1 V, **FIG. 3C** (dark green). When $E^o$ values are more similar, the voltammogram may suggest a single redox centre, for example a single peak with $W_{1/2}$ = 90 mV for two $n$ = 1 centres with identical $E^o$, **FIG. 3C** (purple). In such situations fine structure within non-catalytic peaks may be indicative of multiple overlapping contributions. The ability of multiple half-reactions to describe non-catalytic peaks can be readily assessed by modelling the Faradaic currents using the equations presented above with $E^o$ and $n$ as variables. Such modelling can be performed in a spreadsheet programme or with iterative fitting using QSoas[42-44]. In parallel to such analysis, CV can be performed at a different pH values. $E^o$ of one half-reaction may respond differently to pH, causing multiple, distinct non-catalytic peaks to be resolved for both oxidation and reduction.

The shape of non-catalytic peaks depends on the scan rate, **FIG. 4A**. For half-reactions with the form Ox + $ne^-$ → Red, the descriptions above are relevant at low scan rates, typically <30 mV $s^{-1}$. At higher scan rates, the oxidation and reduction peaks become smeared across the potential axis and peak currents are smaller than predicted by extrapolating values measured at low scan rates, **FIG. 4A**. As the scan rate increases, the peak currents remain approximately equal ($i_p^{ox} \approx |i_p^{red}|$), $E_p^{ox}$ becomes increasingly positive and $E_p^{red}$ increasingly negative. This is because interfacial electron transfer between the protein and WE becomes -slow on voltammetric timescale. The interfacial electron transfer rate constant ($k_{het}^o$) can be extracted from plots of $E_p^{ox}$ and $E_p^{red}$ versus log(scan rate) using procedures[4,58,65] based on an exponential increase of rate with overpotential, Butler-Volmer equation[15], or Marcus theory, which is more appropriate for protein cofactors with low reorganisation energy[20]. Such plots, **FIG. 4B**, are referred to as Trumpet Plots because the deviation of $E_p^{ox}$ and $E_p^{red}$

from $E^o$ has approximately equal magnitude but opposite sign[66]. More complex behaviour[67] is observed for centres, such as flavins, where consecutive $n$ = 1 reactions occur, sometimes separated by a protonation event.

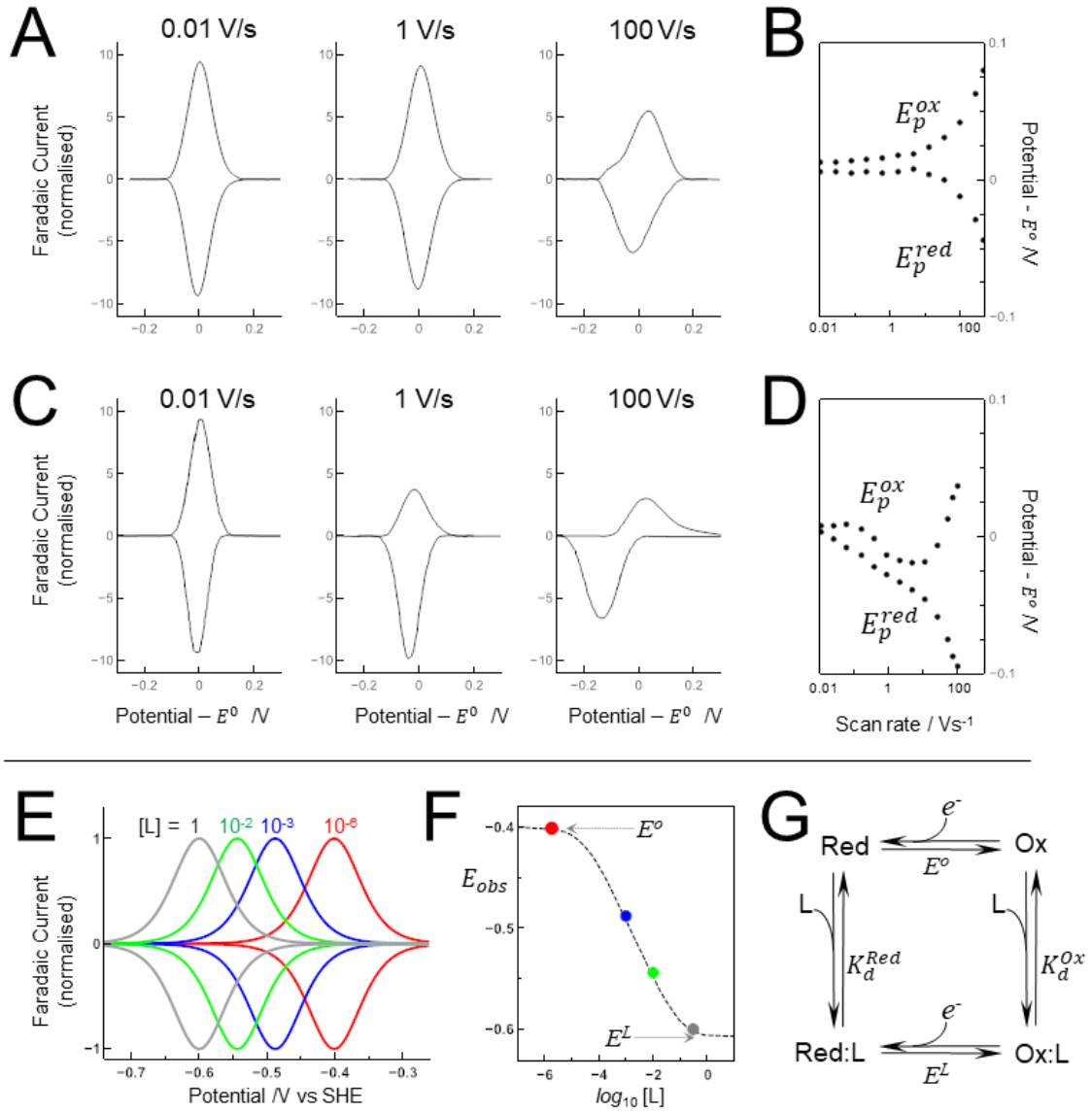


Fig. 4 | **Trumpet plots and ligand binding and unbinding. A**| Faradaic currents from CV at the stated scan rates illustrating behaviour typical for a reversible redox couple. **B**| Plot of peak potentials versus scan rate on a log scale for the experiment in **A**. Symmetrical displacements of $E_p^{ox}$ and $E_p^{red}$ about $E^o$ are indicative of reversible electron transfer uncomplicated by slow redox-driven chemistry. **C**| Faradaic currents from CV at the stated scan rates illustrating behaviour indicative of fast reduction followed by a slower, gated reoxidation due to ligand binding to the reduced protein. **D**| Plot of peak potentials versus scan rate on a log scale for the experiment in **C**. At higher scan rates the displacements of $E_p^{ox}$ and $E_p^{red}$ about $E^o$ are not equal. **E**| Faradaic currents from CV at the stated ligand (L) concentrations illustrating behaviour typical of ligand binding with greater affinity to an oxidised than reduced cofactor. **F**| Variation of $E^{obs}$ for the data in **E** fit to the behaviour predicted for the dissociation constants $K_d^{Ox}$ = 30 µM, $K_d^{Red}$ = 100 mM and a reduction potential ($E^o$) of -0.4 V for a non-ligated $n$ = 1 cofactor. **G**| Square-scheme illustrating ligand binding to an $n$ = 1 redox centre and the corresponding thermodynamic parameters.

***Redox-driven ligand binding and unbinding***

CV provides several ways to identify and characterise redox-driven chemistry, such as ligand binding and unbinding. One approach is to study the scan rate dependence of the non-catalytic peaks and look for change in the relative magnitudes of $i_p^{ox}$ and $i_p^{red}$, **FIG. 4C**[68]. For this example, $i_p^{ox}$ decreases relative to $\left| i_p^{red} \right|$ at higher scan rates. The reduction peak remains well-defined. By contrast, the oxidation peak is increasingly smeared towards more positive potentials. The corresponding plot of $E_p^{ox}$ and $E_p^{red}$ versus log (scan rate) no longer resembles a trumpet, **FIG. 4D**. CV at the higher scan rates reveals that reduction is fast, but re-oxidation is slower. Such behaviour is indicative of a chemical change in the reduced state, which is slow to reverse, limiting the rate of re-oxidation. Using the corresponding reaction scheme (Ox + $ne^-$ ↔ Red ↔ Red*) , rate constants can be quantified by modelling the scan rate dependence of the non-catalytic peaks[20,22,68-71].

A second way to identify ligand binding and unbinding is to study the non-catalytic peaks at low scan rates in solutions of different ligand concentration (for proton binding this is different pH), **FIG. 4E**. For conditions where $i_p^{ox} \approx \left| i_p^{red} \right|$ and $E_p^{ox} \approx E_p^{red}$ the observed reduction potential $E^{\text{obs}} = ( E_p^{ox} + E_p^{red})/2$ is dependent on ligand concentration, **FIG. 4F**. To define the thermodynamic parameters describing ligand binding, the data is fitted to a relevant equation[9,68,69,72]. For example, Equation (4) describes the behaviour for ligand binding to an $n$ = 1 redox site:

*Equation (4)*

$$E^{obs} = E^{o} + \frac{RT}{F} \ln \frac{\left(1 + \frac{[L]}{K_d^{Red}}\right)}{\left(1 + \frac{[L]}{K_d^{Ox}}\right)}$$

where $E^o$ is the reduction potential in the absence of a ligand, [L] is ligand concentration, $K_d^{Ox}$ and $K_d^{Red}$ are dissociation constants for ligand binding to the oxidised and reduced states, respectively, **FIG. 4G**. In the limit that [L] >> $K_d^{Ox}$ and $K_d^{Red}$, the value of $E^{\text{obs}}$ is equal to the reduction potential of the ligand bound redox cofactor, $E^{\text{L}}$, **FIG. 4G**.

Redox-coupled processes can occur on timescales much longer than a single cyclic voltammogram. In this situation, the chemistry and rates can be quantified by recording cyclic voltammetry continuously at a constant scan rate. The appearance of peaks due to the product and disappearance of peaks due to the reactant will be observed [73,74].

***Redox catalysis***

During PFE in the presence of a catalytic substrate, the oxidation state of an adsorbed enzyme changes when the substrate is transformed to product. The WE acts as a redox partner to the enzyme, restoring the initial state of the enzyme, enabling further rounds of catalysis. Electrons are no longer confined to the protein film and a continuous flow of Faradaic current reports the rate of catalysis by the adsorbed film. This Faradaic current is referred to as the catalytic current.

When formation of an oxidised product is irreversible — unidirectional catalysis — and substrate binding depends on prior oxidation of the active site, the fraction of molecules that are oxidised, able to bind a substrate and complete the catalytic cycle is defined by the WE potential through the Nernst equation[75]. The corresponding CV, **FIG. 5A**, reports a sigmoidal increase in positive catalytic current when sweeping from more negative to more positive WE potentials. Similarly, CV of an adsorbed enzyme performing unidirectional reductive catalysis reports a sigmoidal increase in negative catalytic

current on sweeping to more negative WE potentials, **FIG. 5B**. When the catalytic current-potential profiles are independent of scan direction and scan rate (typically < 20 mV $s^{-1}$ in PFE) steady-state catalysis is described through Equation (5)[8,76]:

*Equation (5)*

$$|i_{cat}(E)| = \frac{i_{lim}}{1 + exp\left(\pm\frac{n_{cat}F}{RT}(E_{hw} - E)\right)}$$

Here, $i_{\mathrm{cat}}(E)$ is the catalytic current for WE potential $E$; $i_{lim}$ is the maximum catalytic current magnitude; $i_{lim}^{ox}$ for oxidative catalysis and $i_{lim}^{red}$ for reductive catalysis, **FIG. 5A,B**. $E_{\mathrm{hw}}$ is the half-wave potential, the potential where the current is half of $i_{lim}$; $n_{cat}$ relates to the steepness of the catalytic wave and the bracketed term is positive for oxidation and negative for reduction. The values of $E_{\mathrm{hw}}$ and $n_{\mathrm{cat}}$ reveal the subtleties of redox catalysis, for example, the consequences of redox equilibration through a chain of electron transfer sites, as illustrated in **FIG. 1A**. The value of $i_{lim}$ provides a direct measure of the maximum rate of catalysis by the protein film through the relationship $i_{lim}/F$ = (Coulombs/sec) ÷ (Coulombs/mole $e^-$) = mole $e^-$/sec.

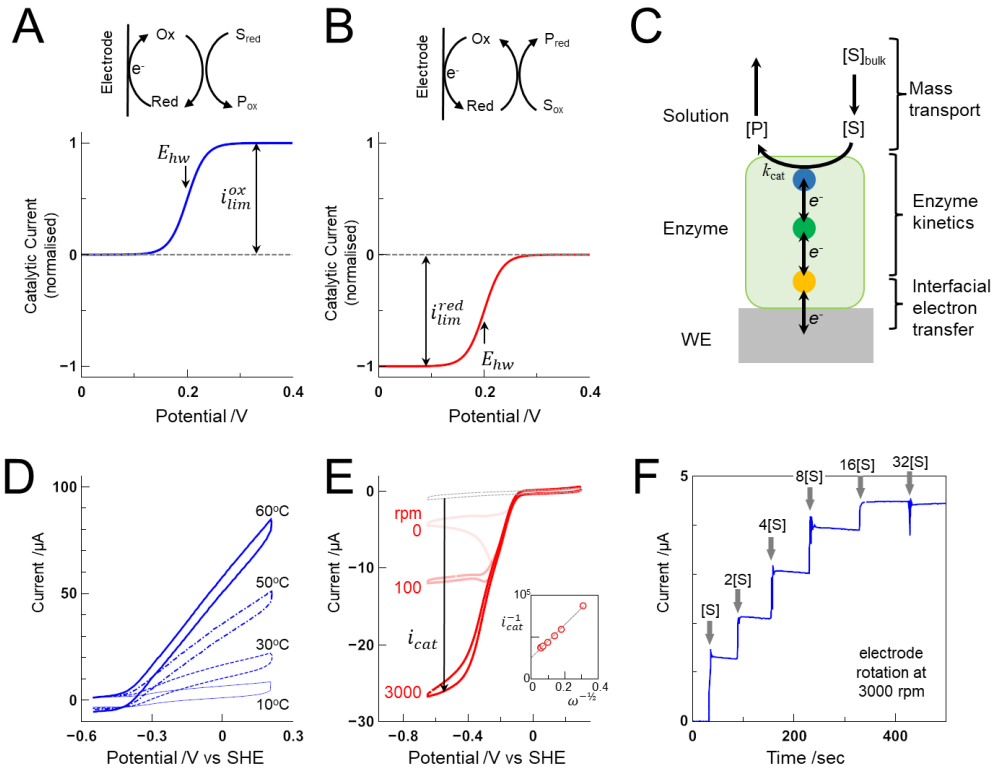


Fig. 5 | **Redox catalysis**. **A**| CV of adsorbed enzyme performing unidirectional oxidation of substrate (S) to product (P). **B**| CV of adsorbed enzyme performing unidirectional substrate reduction. **C**| Schematic illustration of processes that may determine the catalytic rate of an adsorbed enzyme: substrate transport to the electrode, enzyme kinetics ($k_{\mathrm{cat}}$) and interfacial electron transfer. **D**| CV of *A. vinosum* [NiFe] hydrogenase adsorbed on a PGE electrode. Temperature as indicated for 1 atmos. $H_2$, pH 7. Electrode rotation rate 2500 rpm. Scan rate 1 V $s^{-1}$. **E**| CV of *E. coli* cytochrome *c* nitrite reductase adsorbed on a PGE electrode in 130 µM nitrite (red). Electrode rotation at the indicated rates. Scan rate 30 mV $s^{-1}$. CV in the absence of nitrite (grey). Arrow shows measurement of catalytic current ($i_{\mathrm{cat}}$) at -550 mV for the scan towards more negative potential at 3000 rpm. Inset: Koutecky-Levich plot showing 1/($i_{\mathrm{cat}}$ measured at -550 mV) against 1/(angular velocity, $\omega$)$^{1/2}$. **F**| CA for a redox enzyme adsorbed on a PGE electrode rotated at 3000 rpm. Arrows indicate addition of substrate to the electrochemical cell to give the indicated concentration.

PFE of redox catalysis can provide insight into rate defining events intrinsic to the catalytic cycle of the enzyme. These events may be redox transformation of substrate in the active site, substrate binding to the enzyme, or product release from the enzyme. However, before PFE is interpreted in the context of enzyme mechanism, it is important to understand that rate defining events in catalytic PFE may also be defined by interfacial electron transfer, or delivery of substrate to the electrode via mass transport, **FIG. 5C**. Limitations due to slow electron exchange between the WE and protein can be revealed[77] by catalytic currents at high driving force, for instance at WE potentials significantly more negative or positive than the reduction potential of the substrate-product couple. For these potentials, the catalytic current magnitude has residual slope, **FIG. 5D**, instead of a plateau described by $i_{\mathrm{lim}}$, **FIG. 5A,B**. The residual slope arises due to contributions from enzymes with low rates of interfacial electron transfer compared to the enzyme turnover number, $k_{\mathrm{cat}}$. As a result, the slope is greater when enzyme activity is higher. Lowering the temperature, **FIG. 5D**, or substrate concentration can reduce the limitations from slow interfacial electron transfer[77].

Limitations to the catalytic rate from relatively slow substrate delivery to the adsorbed enzyme are readily detected and sometimes overcome with a RDE. The RDE alleviates mass transport limitations by forced convection[15]. Catalytic currents that are free from mass transport limitations will be independent of the electrode rotation rate. When this cannot be achieved experimentally, catalytic currents measured at different rotation rates may be extrapolated to the catalytic current observed at infinitely high electrode rotation rate. This is typically done through a Koutecky-Levich plot with inverse catalytic current versus inverse square root of the rotation rate, presented as angular velocity, **FIG. 5E**[78,79]. Another approach for alleviating diffusion related limitations is to reduce enzyme loading ($\Gamma$) on the electrode surface[80]. This increases the diffusion layer for substrate molecules that reach the enzyme, by allowing hemispherical rather than planar diffusion[81]. Using an ultramicroelectrode as the WE can achieve the same outcome[82,83].

When $i_{lim}$ is defined by the intrinsic properties of the enzyme it can be related to the substrate concentration, [S], through Equation (6), the electrochemical form[8,9,84] of the Michaelis-Menten expression[17] :

*Equation (6)*

$$i_{lim} = \frac{nFA\Gamma k_{cat}[S]}{K_M + [S]}$$

where *n* is the number of electrons needed to convert the substrate to product; $K_M$ is the Michaelis constant; and $k_{cat}$ is the turnover number of the enzyme. Often, the amount of electroactive enzyme, $\Gamma$, is unknown since non-catalytic peaks cannot be discerned. However, the variation of $i_{lim}$ with [S] enables quantification of $K_M$. This is straightforward when there is very little change of $\Gamma$ during an experiment. To check changes in $\Gamma$, the enzyme coated electrode should be returned to standard conditions and $i_{lim}$ remeasured at different time points in the experiment. When a time-dependent decay can be quantified, it is often first order[79,85,86]. $i_{lim}$ can be converted to values at time zero using the first order decay rate and the known time $i_{lim}$ was measured. The time zero currents can be included in Equation (6) to quantify $K_{\mathrm{M}}$. Such approaches are readily extended to assess changes in redox catalysis due to variations in pH and inhibitor concentration. Characteristic changes in $K_{\mathrm{M}}$ and $i_{\mathrm{max}}$ ($\propto k_{\mathrm{cat}}$ for conditions where [S] >> $K_{\mathrm{M}}$) are then interpreted through standard descriptions[17] of enzyme catalysis.

CA provides a powerful complement to CV when studying redox catalysis. Variations in $i_{\mathrm{lim}}$ with substrate or inhibitor concentration can be defined by holding the WE at an appropriate potential and performing sequential additions of the reagent to the electrochemical cell, **FIG. 5F**. During steady-state catalysis, the catalytic current will be constant and independent of time following each addition. When inhibitor addition leads to time-dependent changes, it suggests relatively slow inhibitor binding and unbinding[87-90].

CV can report catalytic currents for both oxidation and reduction. If the adsorbed enzyme catalyses a reaction in both directions — bidirectional catalysis [91,92] — the potential of zero current directly relates to the reduction potential ($E^{o}$) of the substrate-product couple through the Nernst equation[92-94]. Steady-state catalytic current profiles sometimes have additional contributions that describe a boost, or attenuation, of catalysis with increasing driving force. Different explanations have been offered for this behaviour[8].

## APPLICATIONS

Building on the key concepts to interpret PFE and characterise protein redox chemistry, this section provides selected examples that explore these ideas in greater detail. Case studies illustrate how to tailor the WE for direct electron exchange with proteins, the utility of RRDEs, and the benefits of multi-disciplinary studies when interpreting complex non-typical measurements. Examples are presented within a wider discussion of three research areas where PFE is making leading contributions.

### Biosensing

In PFE, the catalytic current for an enzyme-catalysed reaction depends on the substrate concentration, Equation (6). Consequently, PFE can quantify substrate concentration, which underpins the operation of electrochemical biosensors[95-99]. Biosensors operating in this way are sometimes called third generation biosensors. Earlier generations used redox mediators or co-substrates to shuttle electrons between the WE and enzyme. However, small-molecule mediators can diffuse away from the WE during measurements. As a result, electron exchange with the enzyme is compromised and catalytic currents no longer have a simple dependence on the substrate concentration. Biosensors based on direct electron transfer benefit from not requiring redox mediators or co-substrates[96]. The challenge of third generation biosensors is to establish stable electro-active enzyme populations that undergo facile electron transfer with the WE. To address this challenge, different electrode materials and surface functionalization have been explored and a variety of enzymes have been tested for their ability to directly exchange electrons with these electrodes[100-102].

#### *Case Study 1*

Cellobiose dehydrogenase (CDH) is an enzyme that oxidises lactose, providing a basis for electrochemical biosensing of a disaccharide that is prevalent in dairy products and causes symptoms of lactose intolerant. CDH[103] is a monomeric enzyme, **FIG. 6A**, consisting of a catalytic dehydrogenase domain (DH) with strongly a bound flavin adenine dinucleotide in the active site, and a cytochrome domain (CYT) that carries a *b*-type heme. A flexible linker region connects the DH and CYT domains. When CDH is adsorbed on unmodified, solid gold WEs, electrons generated by lactose oxidation in the DH domain are shuttled via CYT to the WE. To improve the long-term stability and catalytic current density of the biosensor, positively charged polyethyleneimine-coated gold nanoparticles (PEI-AuNPs) can be deposited on the WE prior to CDH adsorption[104], **FIG. 6A**. The nanostructured material increases the WE surface area available for enzyme adsorption. In addition, the positively charged PEI

binds and orientates the negatively charged CYT domain to favour direct electron exchange with the WE. CV of CDH adsorbed on PEI-AuNPs, **FIG. 6B**, reports well-defined, reversible peaks due to redox cycling of the *b*-heme in the CYT domain. Variation of the peak potentials with scan rate gives a typical trumpet plot. From this, the rate constant ($k_{het}^{o}$) for electron transfer between CYT and PEI-AuNPs can be calculated as 40 $s^{-1}$. The rate is higher than electron transfer between DH and CYT domains (30 $s^{-1}$), meaning the catalytic oxidation currents measured in the presence of lactose, **FIG. 6C**, are fully determined by the intrinsic properties of the enzyme. Catalytic currents vary linearly with lactose concentrations 1–100 µM, **FIG. 6D**. Fitting to Equation (6) gives a $K_M$ of 0.2 mM lactose. The limit of detection is 0.33 µM lactose. CA establishes that the catalytic currents decrease by only 5.3% during ~300 continuous injections of lactose over 24 hours, indicating excellent long-term stability.

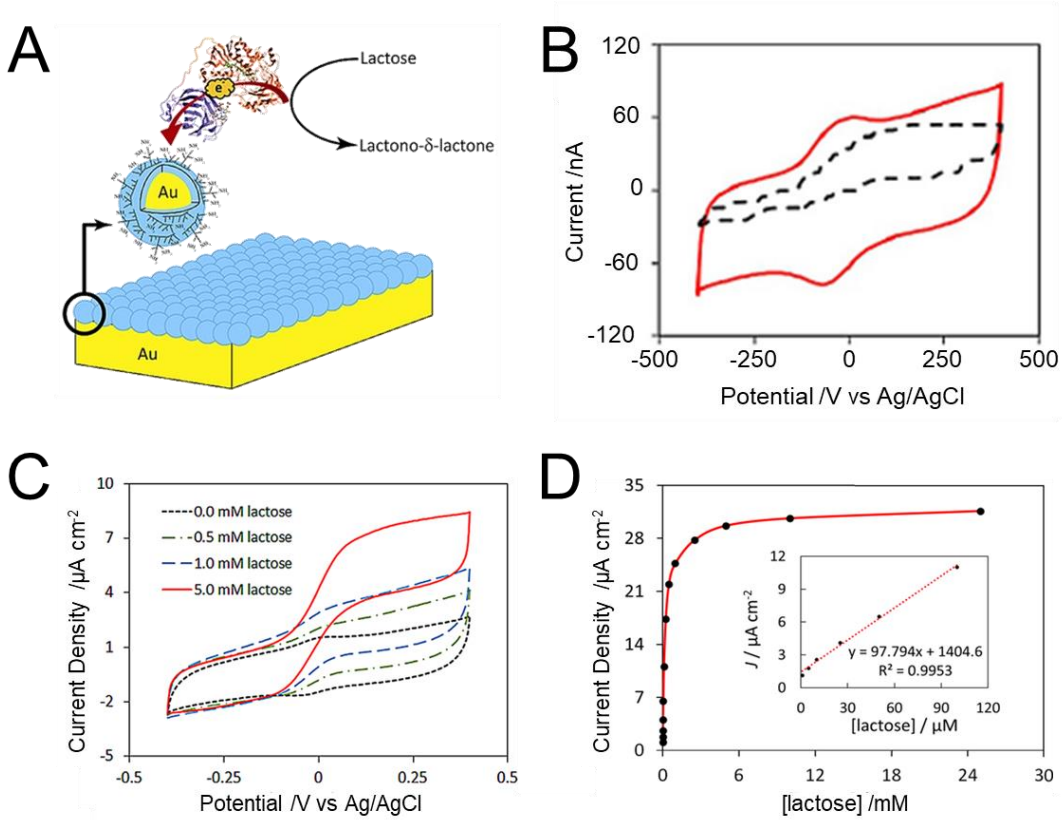


Fig. 6 | **Biosensing. A**| Cartoon illustrating assembly and operation of a lactose biosensor using direct electron transfer between AuNPs and the enzyme CDH. Blue: CYT domain. Red: DH domain. **B**| CV of CDH adsorbed on PEI-AuNPs on a gold WE (red line) and directly on a gold WE (black line) in 5 mM acetate, pH 4.5. Scan rate 1 mV $s^{-1}$. **C**| CV of *Ps*CDH electrostatically immobilized on PEI-AuNPs on a gold WE for the indicated lactose concentrations in 5 mM acetate, pH 4.5. Scan rate 1 mV $s^{-1}$. **D**| Variation of catalytic response with lactose concentration as defined by CA with the WE poised at +250 mV *vs*. Ag/AgCl (0.1 M KCl). Inset: the response in the low-micromolar range.

## Energy conversion

Many redox enzymes evolved to harness energy from the environment, either from sunlight during photosynthesis or chemicals during respiration. PFE replaces an enzyme's natural redox partner with a WE, creating opportunities for sustainable energy conversion. Examples include transfer of chemical to electrical energy in biofuel cells[105,106] and the conversion of light to electricity in biophotovoltaic devices[39,41,52,107]. For converting light to electricity, Photosystem II (PSII) attracts much interest. PSII is a membrane spanning protein complex that produces electrons, oxygen and protons simultaneously via a water-splitting photoreaction[25,108]. PFE readily measures the light-triggered photocurrents

through CA by holding the biophotoelectrode at a desired potential and exposing it to alternating light/dark regimes. Results[109] comparing the WE behaviour with and without immobilized PSII are illustrated in **FIG. 7A**, where PSII was linked to a SAM coated gold WE. The SAM was terminated by nickel-nitrilotriacetic acid functionalities, enabling a direct link to PSII through a polyhistidine-tag. Another approach[110] to immobilize PSII uses electrostatic interactions at ITO WEs, **FIG. 7B**. PSII carries a permanent dipole moment, bringing a positive charge to the region of the protein where electron exchange with the WE occurs. Consequently, ITO WEs coated with a carboxylate (negatively) terminated SAM produces higher photocurrents than equivalent WEs with no SAM or an amine (positively) terminated SAM. Photocurrents can be further enhanced and show greater stability when the carboxylate terminated SAMs incubated with PSII are exposed to covalent coupling molecules, such as carbodiimide and N-hydroxy succinimide.

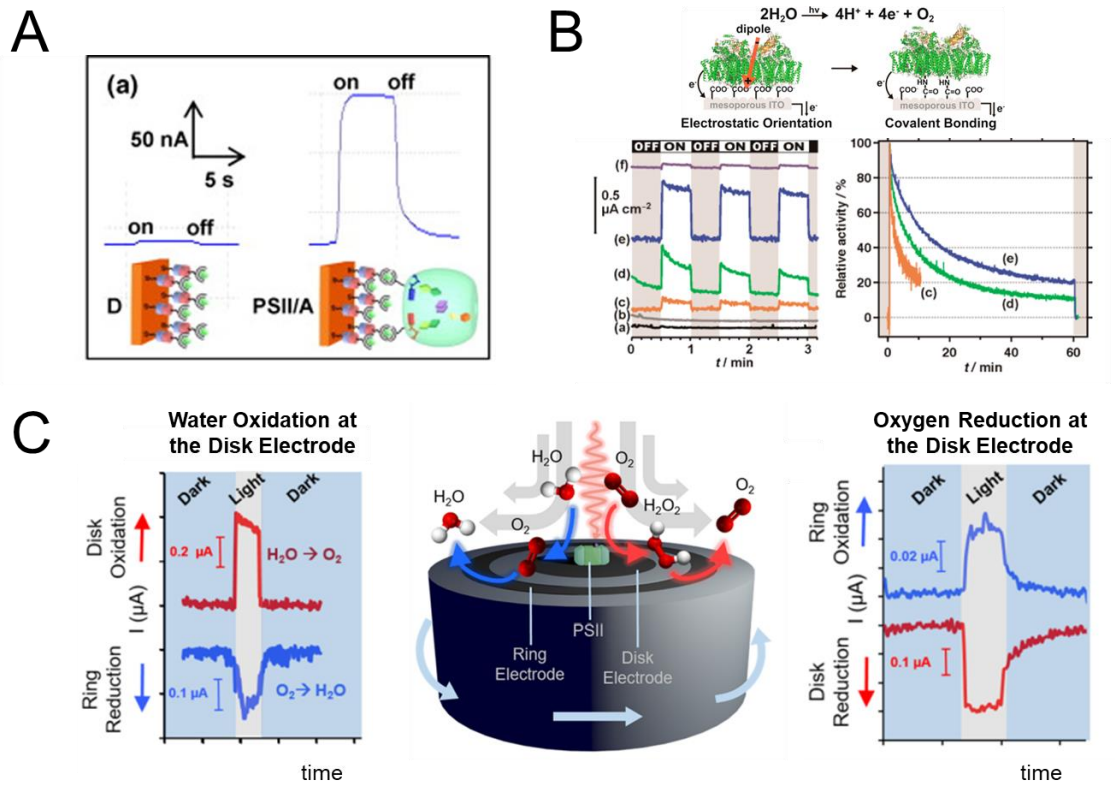


Fig. 7 | **Photoreactivity. A**| CA of a gold WE coated with a SAM terminated by nickel-nitrilotriacetic acid without (left) and with (right) polyhistidine tagged-PSII. WE held at 0.2 V vs. Ag/AgCl (sat. KCl). **B**| Schematic of a mesoporous ITO WE coated with a carboxylate terminated SAM onto which PSII spontaneously adsorbs (top left) and PSII covalently linked to the same electrode by carbodiimide with N-hydroxy succinimide (top right). CA (bottom left) reporting catalytic currents during cycles of irradiation by red-light for mesoporous ITO WEs coated with (a) carboxylate terminated SAM, (b) carboxylate terminated SAM treated with carbodiimide and N-hydroxy succinimide, (c) PSII (d) carboxylate terminated SAM and PSII, (e) carboxylate terminated SAM and PSII followed by exposure to the coupling agents carbodiimide with N-hydroxy succinimide. (f) is a control experiment. CA (bottom right) comparing the catalytic currents during continuous red-light irradiation for electrodes (c–e). WEs poised at +0.5 V vs NHE. **C**| Cartoon of the RRDE setup for studying PSII photochemistry (centre panel). CA revealing $H_2O$ oxidation by PSII at the glassy carbon disk electrode (0.5 V vs SHE) and $O_2$ detection at the Pt ring electrode (-0.5 V vs SHE) (left panel). CA revealing reduction of $O_2$ by PSII at the disk electrode with $H_2O_2$ detected at the ring electrode. Electrode rotation at 400 rpm.

***Case Study 2***

Mechanistic insights into the photoreactivity of PSII by PFE can be achieved using a RRDE[54] and potentiostat to independently control the potential applied at the disk and ring WEs. To study water oxidation, PSII was adsorbed on a glassy carbon disk electrode, **FIG. 7C** (centre) and held at 0.5 V vs SHE in a nitrogen-purged electrolyte solution. Positive photocurrents report light-driven oxidation by PSII, **FIG. 7C** (left red). A platinum ring electrode, held at -0.5 V versus SHE, provides direct quantification of oxygen liberated by PSII as a reductive current, **FIG. 7C** (left blue). Quantifying the photocurrent ratios reveals that the majority (>94%) of electrons delivered to the electrode are used for water oxidation by PSII. A separate experiment performed in the presence of oxygen detected light-driven reduction currents from the PSII coated disk electrode, accompanied by oxidative photocurrents at the ring electrode held at 0.9 V vs SHE **FIG. 7C** (right). Further experiments[54] established two pathways for oxygen reduction to $H_2O_2$ via a PSII generated superoxide ($O_2^{\cdot-}$).

**Elucidating mechanisms of redox catalysis**

Michaelis-Menten descriptors of steady-state redox enzyme catalysis are readily defined by PFE. PFE also provides a powerful route to resolve catalytic mechanisms and properties of catalytic intermediates. For example, CV with substrate concentrations in large excess of $K_M$ enables examination of electron transfer within the enzyme−substrate complex when scan rates are sufficiently fast to outrun the catalytic cycle[111]. For studies of electron transfer within covalent enzyme adducts, the presence of the covalent adduct can be confirmed by mass spectrometry immediately before adsorption on the electrode and on recovery of the sample from the electrode after CV[60].

Arguably, the most significant contributions of PFE to understanding enzyme mechanisms are in dissecting the redox driven activation and deactivation of active centres, and elucidating molecular determinants of substrate access to deeply buried active centres. Such studies highlight how complex behaviours observed by CV as hysteretic catalytic current-potential profiles can be resolved through CA[87,88,112,113]. An illustrative example is the behaviour of *Aquifex aeolicus* NiFe hydrogenase, which catalyses $H_2$ oxidation[88]. The CV, **FIG. 8A**, shows a peak of positive catalytic current corresponding to a maximum $H_2$ oxidation rate. Sweeping to more positive WE potentials increases the rate of $H_2$ oxidation from the active enzyme and simultaneously drives the oxidative formation of inactive enzyme. The activity of the enzyme is recovered by sweeping to more negative potentials, **Fig. 8A**, meaning oxidative inactivation reverses on enzyme reduction. Activation and inactivation are slow on the voltammetric timescale — an experiment at 0.3 mV/s takes about an hour — because the catalytic currents are smaller when sweeping to more negative potentials than when sweeping to more positive potentials. CA exposed the hydrogenase to potentials that inactivated (+65 mV) and then re-activated (-60 mV) the hydrogenase such that the catalytic current decreased and then increased, **FIG. 8B**. Variations in the catalytic current magnitude are directly proportional to the fraction of active enzyme. Rates of activation and deactivation can be quantified by fitting to a scheme that describes the reversible interconversion of active and inactive forms[88].

***Case Study 3***

PFE has contributed to multi-disciplinary studies[89,90,114,115] of CO binding to and inhibition of *Desulfovibrio fructosovorans* NiFe hydrogenase. The crystal structure of this enzyme has a hydrophobic channel that allows $H_2$ from the surrounding solution to diffuse to the NiFe-cofactor containing active site, **FIG. 8C**. The same channel allows CO to reach the active site and act as a competitive inhibitor of $H_2$ oxidation. Insights into how the channel affects CO diffusion rates in the protein were provided by CA of NiFe hydrogenase adsorbed on a rapidly rotating electrode in an

electrochemical cell continuously bubbled with $H_2$ gas[90]. Introducing an aliquot of CO to the enzyme produced immediate inhibition, followed by a slow recovery of activity as CO was flushed out of the electrochemical cell, **FIG. 8D** (left). Gas binding and release rates were calculated from the corresponding amperomograms.

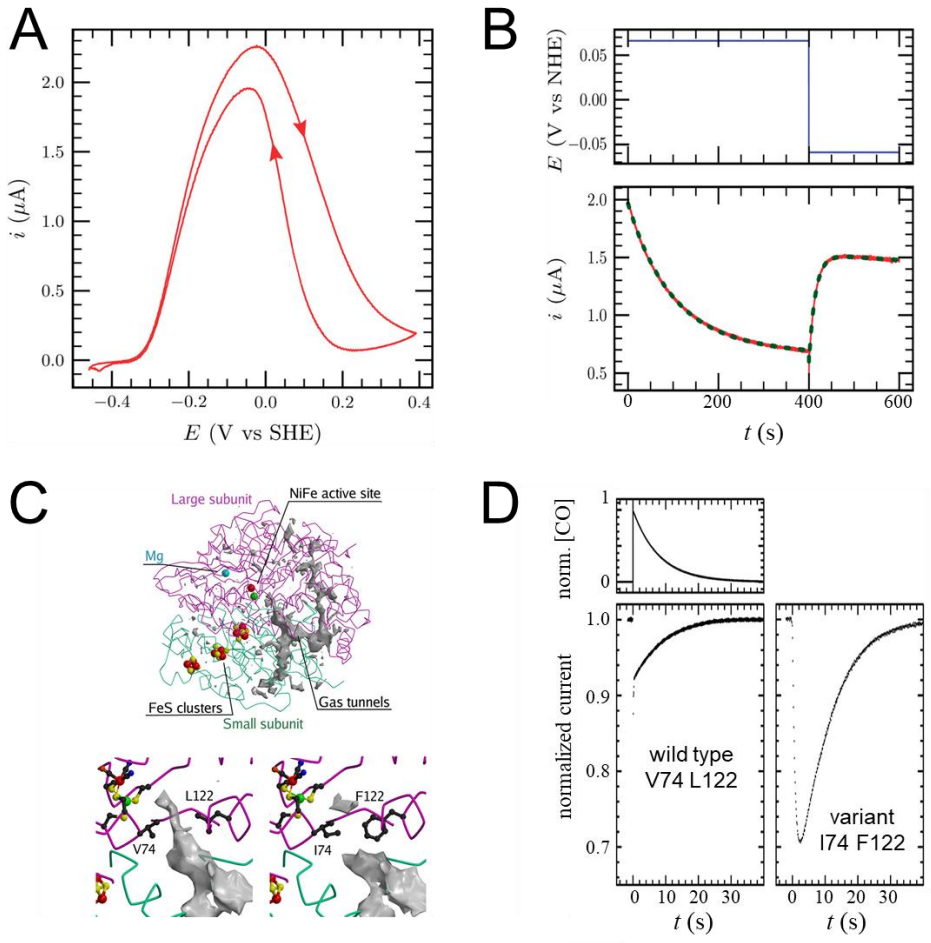


Fig. 8 | **Enzyme mechanism. A**| CV of *A. aeolicus* NiFe hydrogenase adsorbed on a graphite electrode. Electrode rotation rate 4000 rpm, scan rate 0.3 mV $s^{-1}$, pH 7, 40 °C, 1 atm. $H_2$. Arrows indicate the direction of the sweeps. **B**| CA of *A. aeolicus* NiFe hydrogenase. Electrode rotation rate 4000 rpm, pH 8, 40 °C, 1 atm. $H_2$. WE potential against time (upper panel). Catalytic current (red) against time and fit (green) (lower panel). Film loss during measurement accounts for the lower $H_2$ oxidation current at approx. 500 s that at t = 0. **C**| Structure of *D. fructosovorans* NiFe hydrogenase (upper). Detail of the gas tunnel leading to the active site in wild type enzyme (lower left) and the I74, F122 variant (lower right). **D**| CA of *D. fructosovorans* NiFe hydrogenase wild-type enzyme (left) and the L122F-V74I mutant (right) under 1 atmos. $H_2$ and exposed to carbon monoxide (CO) at t = 0. Enzyme adsorbed on a PGE WE. Electrode rotation rate 2000 rpm.

Changing residues Valine74 and Leucine122 in the gas channel to Isoleucine and Phenylalanine respectively, **FIG. 8C**, reduced the CO diffusion rate within the gas channel more than 10-fold[90], **FIG. 8D** (right). The same mutations had minimal impact on the catalytic rate of $H_2$ oxidation, demonstrating that the enzyme may be engineered to resist gaseous inhibition and could be applied as an alternative to platinum catalysts in $H_2$ conversion technology. Furthermore, gas diffusion rates are not simply correlated with the main gas channel width defined by X-ray crystallography, **FIG. 8C**. Molecular dynamics calculations point towards CO diffusion rates being controlled at multiple locations within the gas channel[115].

## REPRODUCIBILITY AND DATA DEPOSITION

For a given protein, reproducibility in PFE relates to the data collected with a single film and from different films. Use of data repositories has not been adopted, but published results are typically available in accord with open access agreements.

Repeatability is related to several factors. PFE for a given protein is critically dependent on instrument parameters, for example, scan rate and vertex potentials for CV, and poising potential and time for CA. The WE rotation rate and temperature may also be defining parameters when studying redox catalysis. If the protein film is prepared on a cold WE, care should be taken to ensure equilibrium occurs at the desired measurement temperature before data collection. Non-reproducible values of $E_p$ and $E_{hw}$ can arise from poorly maintained Res or gas bubbles in the electrochemical cell.

Unwanted and irreproducible contributions can arise from trace amounts of redox active impurities. The method is sensitive, with redox signals visible for quantities < pmol/cm$^2$. All solutions should be carefully defined using water and reagents of the highest possible purity. Careful cleaning of glassware with, for instance, nitric acid, aqua regia, or fuming sulfuric acid is sometimes required to prevent unwanted signals. Protein adsorption may be influenced by co-adsorbing impurities regardless of their redox activity.

For a given sample and measurement condition, variations between separately prepared films include differences in charging current, electroactive coverage and desorption rates. Such discrepancies can be pronounced for different WE treatments. For example, extended application of a certain potential to the electrode can change the electrode surface and protein behaviour. Prolonged poising of the WE after the protein film has formed can also alter the response by changing the state of an enzyme or interface. However, PFE should report the same behaviour when freshly prepared films are subject to an equivalent series of chemical and measurement conditions. For example, values for $E_p$, $W_{½}$ and the ratio $i_p^{ox}/i_p^{red}$ should be consistent for CV that defines redox couples and ligand binding events. During redox catalysis, critical features of the current-potential profile, such as $E_{hw}$ and $n_{cat}$, should be consistent. These parameters can be hard to accurately define when the population of electroactive protein is low, making accurate subtraction of the charging current from the measured current challenging. This challenge is amplified when the baseline deviates significantly from the theoretical behaviour[15] of a plate capacitor. For example, broad peaks due to oxidation or reduction of surface groups are a known complication of working with graphite electrodes. The most appropriate approach to baseline subtraction is still a topic of debate.

PFE will ideally provide the same description of redox chemistry for two or more independently purified samples of a given protein. Unintended and non-reproducible signals can arise from cofactors released from adsorbed or denatured proteins. This is a frequent complication in studies of flavoproteins using graphite electrodes[116]. The extent of adsorption may depend on the presence or identity of an affinity tag introduced to facilitate protein purification[117].

## LIMITATIONS AND OPTIMISATIONS

Not all redox proteins can be studied by PFE. It is essential that the protein has at least one surface exposed redox centre that can act as a point of connection between the electrode and any additional redox centres in the protein, **FIG. 1A**. Establishing conditions to detect and optimise PFE is like finding the conditions for highly ordered protein crystallization ahead of structure resolution by X-ray

diffraction. The chances of success are greater with small, soluble proteins due the high percentage of surface exposed redox cofactors compared to larger proteins.

Most electrode-protein interactions have a contribution from electrostatic interactions. The extent and orientation of protein adsorption can be modulated through changes in the pH and ionic strength of the protein-containing solution, the presence of a co-adsorbate, the choice of WE, and the functional groups in the SAM[118]. If initial experiments have no, or small, Faradaic signals then it is worth exploring different conditions to increase the electroactive population. For studies of redox enzymes, the catalytic currents are proportional to the product of enzyme concentration and turnover number (Equation 6). The chances of success are also increased for highly active enzymes. Because catalytic currents are larger than the corresponding non-catalytic peaks, sometimes by several orders of magnitude, it is always worth adding a substrate to experiments with redox enzymes to look for a catalytic response. Studies of redox catalysis are informative even when there are no detectable non-catalytic peaks.

The WE and composition of the pH buffered electrolyte solution places constraints on the explorable electrochemical potential window. As the majority of PFE is performed in aqueous solution, direct reduction of protons, leading to $H_2$ evolution at the WE, can result in large negative currents that mask currents from the protein of interest. Fortunately, proton reduction is slow at most WE materials specifically mentioned in this account, including gold electrodes with a well-formed SAM. Consequently, the currents appear only at large overpotentials with respect to the $H^+/H_2$ couple. These currents tend to be smaller and appear at more negative potentials for measurements performed at more alkaline pH and faster scan rates. The limiting value of positive potential is typically defined by currents due to oxidation of anions from the electrolyte. It can be altered by changing the concentration or identity of the ions, for instance chloride versus sulphate or chlorate. When using a SAM-coated gold WE, the accessible potential window depends on the identity of the thiol and pH but is typically -0.6 to +1.0 V vs SHE[119,120]. Reductive desorption of the SAM is minimised by using scan rates > 0.1 V/s.

Most PFE experiments aim to uncover the intrinsic properties of proteins relevant to biochemistry. To ensure that the PFE does not arise from a denatured protein or dissociated cofactor, behaviour reported by PFE should correlate with properties observed in complementary measurements[121]. For redox enzymes, $K_M$ values are readily compared to those from the classical biochemical assays. Reduction potentials are typically compared to those defined by potentiometric titration of the protein in solution, although small differences (< 25 mV) can be observed as the environment of an adsorbed protein is not identical to that in solution. The currents measured in PFE report redox activity but do not define the chemical basis of those redox events. To confidently assign a reduction potential to a specific cofactor, and catalytic current to formation of a specific product, information from complementary methods is needed.

## OUTLOOK

PFE has seen continuous developments, with advances in electrode materials, theory, methodology and in situ combination of PFE with spectroscopy and microscopy. Further improvements in these areas will continue to expand the applications of PFE.

For some applications, PFE is limited by low electroactive coverage due to non-optimal protein orientation, poor protein adsorption or because surface exposed redox co-factors are inaccessible for electron exchange with planar macroscopic WEs. These challenges are sometimes overcome by

including conducting nanoparticles, for example carbon nanotubes, graphene oxide flakes, and gold and ITO nanoparticles. Nanoparticles have two important benefits. First, they increase the surface area of the WE, providing more sites for attachment and increasing protein coverage. A second benefit is that nanoparticles enable more interactions with the topologically rich surface of a redox protein. These versatile interactions mean nanoparticles can approach redox centres more closely than planar, macroscopic electrodes.

As shown in Case Study 1[104], **FIG. 6A**, electrodes modified with nanoparticles before protein application can strongly enhance the electroactive coverage. In an alternative approach, protein samples can be mixed with nanoparticles and suspensions applied to the electrode. In the most extreme cases, the protein-nanoparticle composite material can be considered to have become the WE, with the underlying conducting material only used as a connector to the composite material. The resulting higher electroactive coverage has enabled in situ spectroscopy. Examples are hydrogenase studied under turn-over conditions using Fourier transform infrared spectroscopy[122] and redox co-factors characterised at various oxidation states with electron paramagnetic resonance spectroscopy[123] or electronic absorption spectroscopy[48]. Extending the use of spectroscopy in the future will greatly improve the understanding of PFE and expand its applications.

A drawback of using nanoparticle modified WEs when studying redox catalysis — particularly if thick (μm) layers are used with proteins embedded in the nanoparticle layer — is that diffusion of substrates and products through nanoparticle films can be limited. Detailed descriptions of diffusion in such electrodes have yet to be established. However, experimental approaches that facilitate diffusion through nanoparticle layers are being developed. One example is hierarchically structured surfaces with micrometre-sized pores, engineered by templating or printing techniques[38,124]. Further developments to electrode materials will improve adsorption of electroactive protein and access to substrates. Electrocatalytic currents of > 1 mA/cm$^2$ have already been obtained[125,126]. Current densities >> 10 mA/cm$^2$ could make PFE commercially relevant for biosynthesis of fuels and chemicals, but this would require improvements in the stability of the protein films, for example by grafting[127,128] the enzyme to the electrode. New electrochemical theory and models will benefit electrode structure design and further optimization[126].

Protein films in PFE are typically prepared for and used to study one enzyme at a time. However, many interesting metabolic pathways, for example methanogenesis, contain enzyme cascades. The products of PFE, such as NAD(P)H, are high-value substrates for industrially relevant enzymes and biocatalytic reactions. Coupling multiple enzymes on a surface, or trapping them in small compartments on the electrode, will provide new opportunities in biotechnology[129] and to control points within a metabolic pathway[130-132].

For PFE to find widespread applications in biosensing, it is necessary to use reproducible, cheap, and possibly single-use electrodes. Historically, most laboratories used home built WEs, although some electrodes suitable for PFE are now commercially available. This situation is expected to stimulate more research using PFE. Commercially available and affordable single-use electrodes, such as screen-printed electrodes, that support reproducible PFE would benefit applications in biosensing and diagnostics.

There are several classes of proteins that are difficult to study with PFE. The first is membrane proteins, which require detergents to accommodate their amphiphilic nature and prevent aggregation. However, detergent micelles in solution and around the protein can interfere with protein film formation. PFE is possible for membrane proteins with large extramembranous domains and relatively small transmembrane domains [133 134], but is increasingly difficult for complex polytopic

membrane proteins. Electrodes have been designed to accommodate membrane proteins within lipid membranes[135], but imbedding in a lipid membrane influences the orientation of a membrane protein on an electrode surface. New methods, for instance with nanoparticles[136], need to be explored to see how membrane proteins can be studied with PFE.

A second class of oxidoreductases that are difficult to study with PFE are those that have a ping-pong mechanism with active sites buried deep in the enzyme core. An example is glucose oxidase, where oxygen and glucose alternatively bind to an active site flavin adenine dinucleotide (FAD) in the centre of the protein. The relatively long distance between the FAD and protein surface means that direct electron transfer to the WE is strongly impaired and requires special considerations, such as attachment of gold nanoparticles at specific surface sites[137]. There are only a few examples of PFE used to study enzymes with radical intermediates, that undergo thiol-disulphide interconversion, that produce radical oxygen species or that produce radical nitrogen species[138,139]. Developing strategies to interface oxidoreductases with WEs will extend the number of redox proteins and processes that can be studied with PFE.

This manuscript has focussed on CV and CA. However, other techniques have contributed to the development of PFE, notably square-wave voltammetry, differential pulse voltammetry and electrochemical impedance spectroscopy[62,140-142]. Developments in large amplitude sinusoidal voltammetry or Fourier transform alternating current voltammetry have enabled differentiation of various components that contribute to voltametric currents, for instance, non-Faradaic versus Faradaic currents, or catalytic versus non-catalytic currents [138,143,144]. To widen the use of these techniques, they need to become available on commercial potentiostats, with freely accessible software for analysis.

**Acknowledgments.**

JNB and LJCJ thank Professor Fraser Armstrong for inspiring and guiding their introduction to PFE, and the many students and colleagues with whom they have subsequently collaborated in applying and developing the technique. They are grateful for long-term funding from UK Research Councils, notably BBSRC most recently through grants BB/S000704/1 and BB/S002499/1. JAJB is funded by a PhD studentship from the University of East Anglia and ASC by the UKRI Biotechnology and Biological Sciences Research Council Norwich Research Park Biosciences Doctoral Training Partnership [Grant number BB/T008717/1).

**Competing Interests:**

The authors declare no competing interests

**References:**

1 Liu, J. *et al.* Metalloproteins containing cytochrome, iron-sulfur, or copper redox centers. *Chem Rev* **114**, 4366-4469 (2014). https://doi.org:10.1021/cr400479b

2 Lippard, S. J. & Berg, J. M. *Principles of Bioinorganic Chemistry*. (University Science Books, 1994).

3 Moser, C. C., Keske, J. M., Warncke, K., Farid, R. S. & Dutton, P. L. Nature of biological electron transfer. *Nature* **355**, 796-802 (1992). https://doi.org:10.1038/355796a0

4 Armstrong, F. A., Evans, R. M. & Megarity, C. F. Protein film electrochemistry of iron-sulfur enzymes. *Meth Enzymol* **599**, 387-407 (2018). https://doi.org:10.1016/bs.mie.2017.11.001

5 Armstrong, F. A., Heering, H. A. & Hirst, J. Reactions of complex metalloproteins studied by protein-film voltammetry. *Chem Soc Rev* **26**, 169-179 (1997). https://doi.org:10.1039/cs9972600169

6 Armstrong, F. A. & Wilson, G. S. Recent developments in Faradaic bioelectrochemistry. *Electrochim Acta* **45**, 2623-2645 (2000). https://doi.org:10.1016/S0013-4686(00)00342-X

7 del Barrio, M. *et al.* Electrochemical investigations of hydrogenases and other enzymes that produce and use solar fuels. *Acc Chem Res* **51**, 769-777 (2018). https://doi.org:10.1021/acs.accounts.7b00622

8 Leger, C. & Bertrand, P. Direct electrochemistry of redox enzymes as a tool for mechanistic studies. *Chem Rev* **108**, 2379-2438 (2008). https://doi.org:10.1021/cr0680742

9 Hirst, J. Elucidating the mechanisms of coupled electron transfer and catalytic reactions by protein film voltammetry. *BBA-Bioenergetics* **1757**, 225-239 (2006). https://doi.org:10.1016/j.bbabio.2006.04.002

10 Gates, A. J. *et al.* The relationship between redox enzyme activity and electrochemical potential-cellular and mechanistic implications from protein film electrochemistry. *Phys Chem Chem Phys* **13**, 7720-7731 (2011). https://doi.org:10.1039/c0cp02887h

11 Campbell-Rance, D. S., Doan, T. T. & Leopold, M. C. Sweep, step, pulse, and frequency-based techniques applied to protein monolayer electrochemistry at nanoparticle interfaces. *J Electroanal Chem* **662**, 343-354 (2011). https://doi.org:10.1016/j.jelechem.2011.09.005

12 Armstrong, F. A., Butt, J. N., George, S. J., Hatchikian, E. C. & Thomson, A. J. Evidence for reversible multiple redox transformations of [3Fe-4S] clusters. *FEBS Lett* **259**, 15-18 (1989). https://doi.org:10.1016/0014-5793(89)81483-8

13 Feng, Z. Q., Imabayashi, S., Kakiuchi, T. & Niki, K. Electroreflectance spectroscopic study of the electron-transfer rate of cytochrome *c* electrostatically immobilized on the omega-carboxyl alkanethiol monolayer modified gold electrode. *J Electroanal Chem* **394**, 149-154 (1995). https://doi.org:10.1016/0022-0728(95)04058-V

14 Willit, J. L. & Bowden, E. F. Determination of unimolecular electron-transfer rate constants for strongly adsorbed cytochrome *c* on tin oxide electrodes. *J Electroanal Chem* **221**, 265-274 (1987). https://doi.org:10.1016/0022-0728(87)80264-4

15 Bard, A. J. & Faulkner, L. R. *Electrochemical Methods. Fundamentals and Applications.*, (John Wiley & Sons Inc., 2000).

16 Compton, R. & Banks, C. *Understanding Voltammetry* Third Edition edn, (WSPC (Europe), 2018).

17 Nelson, D. L. & Cox, M. M. *Lehninger Principles of Biochemistry*. (W. H. Freeman, 2021).

18 Colburn, A. W., Levey, K. J., O'Hare, D. & Macpherson, J. V. Lifting the lid on the potentiostat: a beginner's guide to understanding electrochemical circuitry and practical operation. *Phys Chem Chem Phys* **23**, 8100-8117 (2021). https://doi.org:10.1039/d1cp00661d

19 Caux, M. *et al.* PassStat, a simple but fast, precise and versatile open source potentiostat. *Hardwarex* **11**, e00290 (2022). https://doi.org:10.1016/j.ohx.2022.e00290

20 Hirst, J. & Armstrong, F. A. Fast-scan cyclic voltammetry of protein films on pyrolytic graphite edge electrodes: Characteristics of electron exchange. *Anal Chem* **70**, 5062-5071 (1998). https://doi.org:10.1021/ac980557l

21 Jeuken, L. J. C., McEvoy, J. P. & Armstrong, F. A. Insights into gated electron-transfer kinetics at the electrode-protein interface: A square wave voltammetry study of the blue copper protein azurin. *J Phys Chem B* **106**, 2304-2313 (2002). https://doi.org:10.1021/jp0134291

22 Hirst, J. *et al.* Kinetics and mechanism of redox-coupled, long-range proton transfer in an iron-sulfur protein. Investigation by fast-scan protein-film voltammetry. *J Am Chem Soc* **120**, 7085-7094 (1998). https://doi.org:10.1021/ja980380c

23 Heering, H. A., Mondal, M. S. & Armstrong, F. A. Using the pulsed nature of staircase cyclic voltammetry to determine interfacial electron-transfer rates of adsorbed species. *Anal Chem* **71**, 174-182 (1999). https://doi.org:10.1021/ac980844p

24 Anantharaj, S. & Noda, S. iR drop correction in electrocatalysis: everything one needs to know! *J Mater Chem A* **10**, 9348-9354 (2022). https://doi.org:10.1039/d2ta01393b

25 Kato, M., Zhang, J. Z., Paul, N. & Reisner, E. Protein film photoelectrochemistry of the water oxidation enzyme photosystem II. *Chem Soc Rev* **43**, 6485-6497 (2014). https://doi.org:10.1039/c4cs00031e

26 Sensi, M. *et al.* Photoinhibition of FeFe hydrogenase. *ACS Catal* **7**, 7378-7387 (2017). https://doi.org:10.1021/acscatal.7b02252

27 Murgida, D. H. In situ spectroelectrochemical investigations of electrode-confined electron-transferring proteins and redox enzymes. *ACS Omega* **6**, 3435-3446 (2021). https://doi.org:10.1021/acsomega.0c05746

28 Jeuken, L. J. C. Structure and modification of electrode materials for protein electrochemistry. *Adv Biochem Eng Biotechnol* **158**, 43-73 (2017). https://doi.org:10.1007/10_2015_5011

29 Sahin, S. & Milton, R. D. Evolving enzymatic electrochemistry with rare or unnatural amino acids. *Curr Opin Electrochem* **35**, 101102 (2022). https://doi.org:10.1016/j.coelec.2022.101102

30 Campbell, W. H., Henig, J. & Plumere, N. Affinity binding via Zinc(II) for controlled orientation and electrochemistry of Histidine-tagged nitrate reductase in self-assembled monolayers. *Bioelectrochem* **93**, 46-50 (2013). https://doi.org:10.1016/j.bioelechem.2012.07.002

31 Baffert, C. *et al.* Covalent attachment of FeFe hydrogenases to carbon electrodes for direct electron transfer. *Anal Chem* **84**, 7999-8005 (2012). https://doi.org:10.1021/ac301812s

32 Holzinger, M., Cosnier, S. & Buzzetti, P. H. M. The versatility of pyrene and its derivatives on $sp^2$ carbon nanomaterials for bioelectrochemical applications. *Synth Met* **292** (2023). https://doi.org:10.1016/j.synthmet.2022.117219

33 Mahouche-Chergui, S., Gam-Derouich, S., Mangeney, C. & Chehimi, M. M. Aryl diazonium salts: a new class of coupling agents for bonding polymers, biomacromolecules and nanoparticles to surfaces. *Chem Soc Rev* **40**, 4143-4166 (2011). https://doi.org:10.1039/c0cs00179a

34 Love, J. C., Estroff, L. A., Kriebel, J. K., Nuzzo, R. G. & Whitesides, G. M. Self-assembled monolayers of thiolates on metals as a form of nanotechnology. *Chem Rev* **105**, 1103-1169 (2005). https://doi.org:10.1021/cr0300789

35 Yan, X. M., Tang, J., Tanner, D., Ulstrup, J. & Xiao, X. X. Direct electrochemical enzyme electron transfer on electrodes modified by self-assembled molecular monolayers. *Catalysts* **10** (2020). https://doi.org:10.3390/catal10121458

36 Doan, T. T., Freeman, M. H., Schmidt, A. R., Nguyen, N. D. T. & Leopold, M. C. Synthesis, assembly, and characterization of monolayer protected gold nanoparticle films for protein monolayer electrochemistry. *JoVE*, e3441 (2011). https://doi.org:10.3791/3441

37 Oviedo-Rouco, S. *et al.* Correlated electric field modulation of electron transfer parameters and the access to alternative conformations of multifunctional cytochrome *c*. *Bioelectrochem* **143**, 107956 (2022). https://doi.org:10.1016/j.bioelechem.2021.107956

38 Mersch, D. *et al.* Wiring of Photosystem II to hydrogenase for photoelectrochemical water splitting. *J Am Chem Soc* **137**, 8541-8549 (2015). https://doi.org:10.1021/jacs.5b03737

39 Morlock, S., Subramanian, S. K., Zouni, A. & Lisdat, F. Closing the green gap of photosystem I with synthetic fluorophores for enhanced photocurrent generation in photobiocathodes. *Chem Sci* **14**, 1696-1708 (2023). https://doi.org:10.1039/d2sc05324a

40 Siritanaratkul, B. *et al.* Transfer of photosynthetic NADP(+)/NADPH recycling activity to a porous metal oxide for highly specific, electrochemically-driven organic synthesis. *Chem Sci* **8**, 4579-4586 (2017). https://doi.org:10.1039/c7sc00850c

41 Morlock, S., Subramanian, S. K., Zouni, A. & Lisdat, F. Bio-inorganic hybrid structures for direct electron transfer to photosystem I in photobioelectrodes. *Biosens Bioelectron* **214**, 114495 (2022). https://doi.org:10.1016/j.bios.2022.114495

42 Fourmond, V. QSoas: a versatile software for data analysis. *Anal Chem* **88**, 5050-5052 (2016). https://doi.org:10.1021/acs.analchem.6b00224

43 Merrouch, M., Hadj-Said, J., Leger, C., Dementin, S. & Fourmond, V. Reliable estimation of the kinetic parameters of redox enzymes by taking into account mass transport towards rotating electrodes in protein film voltammetry experiments. *Electrochim Acta* **245**, 1059-1064 (2017). https://doi.org:10.1016/j.electacta.2017.03.114

44 Fourmond, V. & Leger, C. Modelling the voltammetry of adsorbed enzymes and molecular catalysts. *Curr Opin Electrochem* **1**, 110-120 (2017). https://doi.org:10.1016/j.coelec.2016.11.002

45 Heering, H. A., Wiertz, F. G. M., Dekker, C. & de Vries, S. Direct immobilization of native yeast Iso-1 cytochrome *c* on bare gold: Fast electron relay to redox enzymes and zeptomole protein-film voltammetry. *J Am Chem Soc* **126**, 11103-11112 (2004). https://doi.org:10.1021/ja046737w

46 Wang, M. K., Zhao, F., Liu, Y. & Dong, S. J. Direct electrochemistry of microperoxidase at Pt microelectrodes modified with carbon nanotubes. *Biosens Bioelectron* **21**, 159-166 (2005). https://doi.org:10.1016/j.bios.2004.08.012

47 Lockwood, C. W. J. *et al.* Resolution of key roles for the distal pocket histidine in cytochrome *c* nitrite reductases. *J Am Chem Soc* **137**, 3059-3068 (2015). https://doi.org:10.1021/ja512941j

48 Marritt, S. J. *et al.* Spectroelectrochemical characterization of a pentaheme cytochrome in solution and as electrocatalytically active films on nanocrystalline metal-oxide electrodes. *J Am Chem Soc* **130**, 8588-8589 (2008). https://doi.org:10.1021/ja802641a

49 Reuillard, B. *et al.* High performance reduction of $H_2O_2$ with an electron transport decaheme cytochrome on a porous ITO electrode. *J Am Chem Soc* **139**, 3324-3327 (2017). https://doi.org:10.1021/jacs.6b12437

50 Ash, P. A., Hidalgo, R. & Vincent, K. A. Protein film infrared electrochemistry demonstrated for study of $H_2$ oxidation by a [NiFe] hydrogenase. *JoVE*, e55858 (2017). https://doi.org:10.3791/55858

51 Chung, M. W. *et al.* Infrared spectroscopy coupled with protein film electrochemistry to study hydrogenase inhibition by pi-acid ligands. *J Biol Inorg Chem* **19**, S879-S879 (2014).

52 Kornienko, N. *et al.* Advancing techniques for investigating the enzyme-electrode interface. *Acc Chem Res* **52**, 1439-1448 (2019). https://doi.org:10.1021/acs.accounts.9b00087

53 McEvoy, J. P. & Armstrong, F. A. Protein film cryovoltammetry: demonstrations with a 7Fe ([3Fe-4S]+[4Fe-4S]) ferredoxin. *Chem Commun*, 1635-1636 (1999). https://doi.org:10.1039/a903222c

54 Kornienko, N. *et al.* Oxygenic photoreactivity in Photosystem II studied by rotating ring disk electrochemistry. *J Am Chem Soc* **140**, 17923-17931 (2018). https://doi.org:10.1021/jacs.8b08784

55 Fourmond, V. & Leger, C. Protein electrochemistry: questions and answers. *Adv Biochem Eng Biot* **158**, 1-41 (2017). https://doi.org:10.1007/10_2015_5016

56 Hartshorne, R. S. *et al.* Characterization of *Shewanella oneidensis* MtrC: a cell-surface decaheme cytochrome involved in respiratory electron transport to extracellular electron acceptors. *J Biol Inorg Chem* **12**, 1083-1094 (2007). https://doi.org:10.1007/s00775-007-0278-y

57 van Wonderen, J. H., Burlat, B., Richardson, D. J., Cheesman, M. R. & Butt, J. N. The nitric oxide reductase activity of cytochrome *c* nitrite reductase from *Escherichia coli*. *J Biol Chem* **283**, 9587-9594 (2008). https://doi.org:10.1074/jbc.M709090200

58 Laviron, E. General expression of the linear potential sweep voltammogram in the case of diffusionless electrochemical systems. *J Electroanal Chem* **101**, 19-28 (1979). https://doi.org:10.1016/S0022-0728(79)80075-3

59 Plichon, V. & Laviron, E. Theoretical study of a two-step reversible electrochemical reaction associated with irreversible chemical reactions in thin layer linear potential sweep voltammetry. *J. Electroanal. Chem.* **71**, 143-156 (1976). https://doi.org:10.1016/S0022-0728(76)80030-7

60 Jenner, L. P. *et al.* Reaction of thiosulfate dehydrogenase with a substrate mimic induces dissociation of the cysteine heme ligand giving insights into the mechanism of oxidative catalysis. *J Am Chem Soc* (2022). https://doi.org:10.1021/jacs.2c06062

61 Maiocco, S. J., Arcinas, A. J., Booker, S. J. & Elliott, S. J. Parsing redox potentials of five ferredoxins found within *Thermotoga maritima*. *Protein Sci* **28**, 257-266 (2019). https://doi.org:10.1002/pro.3547

62 Zhu, W. *et al.* Structural properties and catalytic implications of the SPASM domain iron-sulfur clusters in *Methylorubrum extorquens* PqqE. *J Am Chem Soc* **142**, 12620-12634 (2020). https://doi.org:10.1021/jacs.0c02044

63 Rizzolo, K. *et al.* A widely distributed diheme enzyme from *Burkholderia* that displays an atypically stable bis-Fe(IV) state. *Nat Commun* **10**, 1101 (2019). https://doi.org:10.1038/s41467-019-09020-4

64 Walker, L. M., Kincannon, W. M., Bandarian, V. & Elliott, S. J. Deconvoluting the reduction potentials for the three [4Fe-4S] clusters in an adoMet radical SCIFF maturase. *Biochemistry* **57**, 6050-6053 (2018). https://doi.org:10.1021/acs.biochem.8b00846

65 Armstrong, F. A. *et al.* Fast, long-range electron-transfer reactions of a 'blue' copper protein coupled non-covalently to an electrode through a stilbenyl thiolate monolayer. *Chem Commun*, 316-317 (2004). https://doi.org:10.1039/b312936e

66 Zitare, U. A. *et al.* The role of molecular crowding in long-range metalloprotein electron transfer: Dissection into site- and scaffold-specific contributions. *Electrochim Acta* **294**, 117-125 (2019). https://doi.org:10.1016/j.electacta.2018.10.069

67 Gulaboski, R., Kokoskarova, P. & Mitrev, S. Theoretical aspects of several successive two-step redox mechanisms in protein-film cyclic staircase voltammetry. *Electrochim Acta* **69**, 86-96 (2012). https://doi.org:10.1016/j.electacta.2012.02.086

68 Shen, B. H. *et al. Azotobacter vinelandii* ferredoxin I. Aspartate-15 facilitates proton transfer to the reduced [3Fe-4S] cluster. *J Biol Chem* **268**, 25928-25939 (1993). https://doi.org:10.1016/S0021-9258(19)74476-7

69 Butt, J. N. *et al.* Voltammetric characterization of rapid and reversible binding of an exogenous thiolate ligand at a [4Fe-4S] cluster in Ferredoxin III from *Desulfovibrio africanus*. *J Am Chem Soc* **115**, 1413-1421 (1993). https://doi.org:10.1021/ja00057a026

70 Hirst, J., Jameson, G. N. L., Allen, J. W. A. & Armstrong, F. A. Very rapid, cooperative two-electron/two-proton redox reactions of [3Fe-4S] clusters: Detection and analysis by protein-film voltammetry. *J Am Chem Soc* **120**, 11994-11999 (1998). https://doi.org:10.1021/ja981693a

71 Camba, R. *et al.* Mechanisms of redox-coupled proton transfer in proteins: Role of the proximal proline in reactions of the [3Fe-4S] cluster in *Azotobacter vinelandii* ferredoxin I. *Biochemistry* **42**, 10589-10599 (2003). https://doi.org:10.1021/bi035021v

72 Steensma, E., Heering, H. A., Hagen, W. R. & vanMierlo, C. P. M. Redox properties of wild-type, Cys69Ala, and Cys69Ser *Azotobacter vinelandii* flavodoxin II as measured by cyclic voltammetry and EPR spectroscopy. *Eur J Biochem* **235**, 167-172 (1996). https://doi.org:10.1111/j.1432-1033.1996.00167.x

73 Butt, J. N., Fawcett, S. E. J., Breton, J., Thomson, A. J. & Armstrong, F. A. Electrochemical potential and pH dependences of [3Fe-4S]<->[M3Fe-4S] cluster transformations (M = Fe, Zn, Co, and Cd) in ferredoxin III from *Desulfovibrio africanus* and detection of a cluster with M = Pb. *J Am Chem Soc* **119**, 9729-9737 (1997). https://doi.org:10.1021/ja971403a

74 Butt, J. N., Niles, J., Armstrong, F. A., Breton, J. & Thomson, A. J. Formation and properties of a stable high-potential copper-iron-sulfur cluster in a ferredoxin. *Nat Struct Biol* **1**, 427-433 (1994). https://doi.org:10.1038/nsb0794-427

75 Heering, H. A., Hirst, J. & Armstrong, F. A. Interpreting the catalytic voltammetry of electroactive enzymes adsorbed on electrodes. *J Phys Chem B* **102**, 6889-6902 (1998). https://doi.org:10.1021/jp981023r

76 Heering, H. A., Weiner, J. H. & Armstrong, F. A. Direct detection and measurement of electron relays in a multicentered enzyme: voltammetry of electrode-surface films of *E. coli* fumarate reductase, an iron-sulfur flavoprotein. *J Am Chem Soc* **119**, 11628-11638 (1997). https://doi.org:10.1021/ja9723242

77 Leger, C., Jones, A. K., Albracht, S. P. J. & Armstrong, F. A. Effect of a dispersion of interfacial electron transfer rates on steady state catalytic electron transport in [NiFe]-hydrogenase and other enzymes. *J Phys Chem B* **106**, 13058-13063 (2002). https://doi.org:10.1021/jp0265687

78 Sucheta, A., Cammack, R., Weiner, J. & Armstrong, F. A. Reversible electrochemistry of fumarate reductase immobilized on an electrode surface - direct voltammetric observations of redox centers and their participation in rapid catalytic electron-transport. *Biochemistry* **32**, 5455-5465 (1993). https://doi.org:10.1021/bi00071a023

79 Angove, H. C., Cole, J. A., Richardson, D. J. & Butt, J. N. Protein film voltammetry reveals distinctive fingerprints of nitrite and hydroxylamine reduction by a cytochrome c nitrite reductase. *J Biol Chem* **277**, 23374-23381 (2002). https://doi.org:10.1074/jbc.M200495200

80 Jones, A. K., Sillery, E., Albracht, S. P. J. & Armstrong, F. A. Direct comparison of the electrocatalytic oxidation of hydrogen by an enzyme and a platinum catalyst. *Chem Commun*, 866-867 (2002). https://doi.org:10.1039/b201337a

81 Armstrong, F. A. *et al.* Electrocatalytic reduction of hydrogen-peroxide at a stationary pyrolytic-graphite electrode surface in the presence of cytochrome *c* peroxidase - a description based on a microelectrode array model for adsorbed enzyme molecules. *Analyst* **118**, 973-978 (1993). https://doi.org:10.1039/an9931800973

82 Hoeben, F. J. M. *et al.* Polymyxin-coated Au and carbon nanotube electrodes for stable [NiFe]-hydrogenase film voltammetry. *Langmuir* **24**, 5925-5931 (2008). https://doi.org:10.1021/la703984z

83 Armstrong, F. A. Recent developments in dynamic electrochemical studies of adsorbed enzymes and their active sites. *Curr Opin Chem Biol* **9**, 110-117 (2005). https://doi.org:10.1016/j.cbpa.2005.02.011

84 Leger, C. *et al.* Enzyme electrokinetics: Energetics of succinate oxidation by fumarate reductase and succinate dehydrogenase. *Biochemistry* **40**, 11234-11245 (2001). https://doi.org:10.1021/bi010889b

85 Anderson, L. J., Richardson, D. J. & Butt, J. N. Catalytic protein film voltammetry from a respiratory nitrate reductase provides evidence for complex electrochemical modulation of enzyme activity. *Biochemistry* **40**, 11294-11307 (2001). https://doi.org:10.1021/bi002706b

86 Fourmond, V. *et al.* Correcting for electrocatalyst desorption and inactivation in chronoamperometry experiments. *Anal Chem* **81**, 2962-2968 (2009). https://doi.org:10.1021/ac8025702

87 Gwyer, J. D., Richardson, D. J. & Butt, J. N. Resolving complexity in the interactions of redox enzymes and their inhibitors: Contrasting mechanisms for the inhibition of a cytochrome *c* nitrite reductase revealed by protein film voltammetry. *Biochemistry* **43**, 15086-15094 (2004). https://doi.org:10.1021/bi049085x

88 Fourmond, V., Infossi, P., Giudici-Orticoni, M. T., Bertrand, P. & Leger, C. "Two-step" chronoamperometric method for studying the anaerobic inactivation of an oxygen tolerant NiFe hydrogenase. *J Am Chem Soc* **132**, 4848-4857 (2010). https://doi.org:10.1021/ja910685j

89 Leger, C., Dementin, S., Bertrand, P., Rousset, M. & Guigliarelli, B. Inhibition and aerobic inactivation kinetics of *Desulfovibrio fructosovorans* NiFe hydrogenase studied by protein film voltammetry. *J Am Chem Soc* **126**, 12162-12172 (2004). https://doi.org:10.1021/ja046548d

90 Leroux, F. *et al.* Experimental approaches to kinetics of gas diffusion in hydrogenase. *P Natl Acad Sci USA* **105**, 11188-11193 (2008). https://doi.org:10.1073/pnas.0803689105

91 Fourmond, V., Plumere, N. & Leger, C. Reversible catalysis. *Nat Rev Chem* **5**, 348-360 (2021). https://doi.org:10.1038/s41570-021-00268-3

92 Fourmond, V., Wiedner, E. S., Shaw, W. J. & Leger, C. Understanding and design of bidirectional and reversible catalysts of multielectron, multistep reactions. *J Am Chem Soc* **141**, 11269-11285 (2019). https://doi.org:10.1021/jacs.9b04854

93 Armstrong, F. A. & Hirst, J. Reversibility and efficiency in electrocatalytic energy conversion and lessons from enzymes. *P Natl Acad Sci USA* **108**, 14049-14054 (2011). https://doi.org:10.1073/pnas.1103697108

94 Kurth, J. M., Dahl, C. & Butt, J. N. Catalytic protein film electrochemistry provides a direct measure of the tetrathionate/thiosulfate reduction potential. *J Am Chem Soc* **137**, 13232-13235 (2015). https://doi.org:10.1021/jacs.5b08291

95 Wu, Y. H. & Hu, S. S. Biosensors based on direct electron transfer in redox proteins. *Microchim Acta* **159**, 1-17 (2007). https://doi.org:10.1007/s00604-007-0749-4

96 Das, P., Das, M., Chinnadayyala, S. R., Singha, I. M. & Goswami, P. Recent advances on developing 3rd generation enzyme electrode for biosensor applications. *Biosens Bioelectron* **79**, 386-397 (2016). https://doi.org:10.1016/j.bios.2015.12.055

97 Zuccarello, L., Barbosa, C., Todorovic, S. & Silveira, C. M. Electrocatalysis by heme enzymes-applications in biosensing. *Catalysts* **11** (2021). https://doi.org:10.3390/catal11020218

98 Gulaboski, R., Mirceski, V., Bogeski, I. & Hoth, M. Protein film voltammetry: electrochemical enzymatic spectroscopy. A review on recent progress. *J Solid State Electrochem* **16**, 2315-2328 (2012). https://doi.org:10.1007/s10008-011-1397-5

99 Ronkainen, N. J., Halsall, H. B. & Heineman, W. R. Electrochemical biosensors. *Chem Soc Rev* **39**, 1747-1763 (2010). https://doi.org:10.1039/b714449k

100 Sassolas, A., Blum, L. J. & Leca-Bouvier, B. D. Immobilization strategies to develop enzymatic biosensors. *Biotechnol Adv* **30**, 489-511 (2012). https://doi.org:10.1016/j.biotechadv.2011.09.003

101 Datta, S., Christena, L. R. & Rajaram, Y. R. S. Enzyme immobilization: an overview on techniques and support materials. *3 Biotech* **3**, 1-9 (2013). https://doi.org:10.1007/s13205-012-0071-7

102 Bollella, P. & Katz, E. Enzyme-based biosensors: tackling electron transfer issues. *Sensors* **20** (2020). https://doi.org:10.3390/s20123517

103 Tan, T. C. *et al.* Structural basis for cellobiose dehydrogenase action during oxidative cellulose degradation. *Nat Commun* **6** (2015). https://doi.org:10.1038/ncomms8542

104 Tavahodi, M. *et al.* Direct electron transfer of cellobiose dehydrogenase on positively charged polyethyleneimine gold nanoparticles. *ChemPlusChem* **82**, 546-552 (2017). https://doi.org:10.1002/cplu.201600453

105 Chen, H. *et al.* Fundamentals, applications, and future directions of bioelectrocatalysis. *Chem Rev* **120**, 12903-12993 (2020). https://doi.org:10.1021/acs.chemrev.0c00472

106 Xiao, X. X. *et al.* Tackling the challenges of enzymatic (bio)fuel cells. *Chem Rev* **119**, 9509-9558 (2019). https://doi.org:10.1021/acs.chemrev.9b00115

107 Noll, T. & Noll, G. Strategies for "wiring" redox-active proteins to electrodes and applications in biosensors, biofuel cells, and nanotechnology. *Chem Soc Rev* **40**, 3564-3576 (2011). https://doi.org:10.1039/c1cs15030h

108 Zhang, J. Z. & Reisner, E. Advancing photosystem II photoelectrochemistry for semi-artificial photosynthesis. *Nat Rev Chem* **4**, 6-21 (2020). https://doi.org:10.1038/s41570-019-0149-4

109 Terasaki, N. *et al.* Photocurrent generation properties of Histag-photosystem II immobilized on nanostructured gold electrode. *Thin Solid Films* **516**, 2553-2557 (2008). https://doi.org:10.1016/j.tsf.2007.04.127

110 Kato, M., Cardona, T., Rutherford, A. W. & Reisner, E. Covalent immobilization of oriented Photosystem II on a nanostructured electrode for solar water oxidation. *J Am Chem Soc* **135**, 10610-10613 (2013). https://doi.org:10.1021/ja404699h

111 Jones, A. K., Camba, R., Reid, G. A., Chapman, S. K. & Armstrong, F. A. Interruption and time-resolution of catalysis by a flavoenzyme using fast scan protein film voltammetry. *J Am Chem Soc* **122**, 6494-6495 (2000). https://doi.org:10.1021/ja000848n

112 Orain, C. *et al.* Electrochemical measurements of the kinetics of inhibition of two FeFe Hydrogenases by $O_2$ demonstrate that the reaction Is partly reversible. *J Am Chem Soc* **137**, 12580-12587 (2015). https://doi.org:10.1021/jacs.5b06934

113 Field, S. J. *et al.* Reductive activation of nitrate reductases. *Dalton Trans*, 3580-3586 (2005). https://doi.org:10.1039/b505530j

114 Liebgott, P. P. *et al.* Relating diffusion along the substrate tunnel and oxygen sensitivity in hydrogenase. *Nat Chem Biol* **6**, 63-70 (2010). https://doi.org:10.1038/Nchembio.276

115 Wang, P. H. & Blumberger, J. Mechanistic insight into the blocking of CO diffusion in [NiFe]-hydrogenase mutants through multiscale simulation. *P Natl Acad Sci USA* **109**, 6399-6404 (2012). https://doi.org:10.1073/pnas.1121176109

116 Heering, H. A. & Hagen, W. R. Complex electrochemistry of flavodoxin at carbon-based electrodes: Results from a combination of direct electron transfer, flavin-mediated electron transfer and comproportionation. *J Electroanal Chem* **404**, 249-260 (1996). https://doi.org:10.1016/0022-0728(95)04248-2

117 Hwang, E. T. *et al.* Exploring step-by-step assembly of nanoparticle: cytochrome biohybrid photoanodes. *ChemElectroChem* **4**, 1959-1968 (2017). https://doi.org:10.1002/celc.201700030

118 Badiani, V. M. *et al.* Elucidating film loss and the role of hydrogen bonding of adsorbed redox enzymes by electrochemical quartz crystal microbalance analysis. *ACS Catal* **12**, 1886-1897 (2022). https://doi.org:10.1021/acscatal.1c04317

119 Beulen, M. W. J., Kastenberg, M. I., van Veggel, F. C. J. M. & Reinhoudt, D. N. Electrochemical stability of self-assembled monolayers on gold. *Langmuir* **14**, 7463-7467 (1998). https://doi.org:10.1021/la981031z

120 Ramos, N. C., Medlin, J. W. & Holewinski, A. Electrochemical stability of thiolate self-assembled monolayers on Au, Pt, and Cu. *ACS Appl Mater Interfaces* **15**, 14470-14480 (2023). https://doi.org:10.1021/acsami.3c01224

121 Milton, R. D. & Minteer, S. D. Direct enzymatic bioelectrocatalysis: differentiating between myth and reality. *J R Soc Interface* **14**, 20170253 (2017). https://doi.org:10.1098/rsif.2017.0253

122 Ash, P. A., Kendall-Price, S. E. T. & Vincent, K. A. Unifying activity, structure, and spectroscopy of [NiFe] hydrogenases: combining techniques to clarify mechanistic understanding. *Acc Chem Res* **52**, 3120-3131 (2019). https://doi.org:10.1021/acs.accounts.9b00293

123 Abdiaziz, K., Salvadori, E., Sokol, K. P., Reisner, E. & Roessler, M. M. Protein film electrochemical EPR spectroscopy as a technique to investigate redox reactions in biomolecules. *Chem Commun* **55**, 8840-8843 (2019). https://doi.org:10.1039/c9cc03212f

124 Chen, X. L. *et al.* 3D-printed hierarchical pillar array electrodes for high-performance semi-artificial photosynthesis. *Nat Mater* **21**, 811-818 (2022). https://doi.org:10.1038/s41563-022-01205-5

125 Liu, Y. P. *et al.* Facile functionalization of carbon electrodes for efficient electroenzymatic hydrogen production. *JACS Au* **3**, 124-130 (2023). https://doi.org:10.1021/jacsau.2c00551

126 Moore, E. E. *et al.* Understanding the local chemical environment of bioelectrocatalysis. *P Natl Acad Sci USA* **119**, e2114097119 (2022). https://doi.org:10.1073/pnas.2114097119

127 Alonso-Lomillo, M. A. *et al.* Hydrogenase-coated carbon nanotubes for efficient $H_2$ oxidation. *Nano Lett* **7**, 1603-1608 (2007). https://doi.org:10.1021/nl070519u

128 Rudiger, O., Abad, J. M., Hatchikian, E. C., Fernandez, V. M. & De Lacey, A. L. Oriented immobilization of *Desulfovibrio gigas* hydrogenase onto carbon electrodes by covalent bonds for nonmediated oxidation of $H_2$. *J Am Chem Soc* **127**, 16008-16009 (2005). https://doi.org:10.1021/ja0554312

129 Yarman, A. *et al.* Third generation ATP sensor with enzymatic analyte recycling. *Electroanal* **26**, 2043-2048 (2014). https://doi.org:10.1002/elan.201400231

130 Armstrong, F. A., Cheng, B. C., Herold, R. A., Megarity, C. F. & Siritanaratkul, B. From protein film electrochemistry to nanoconfined enzyme cascades and the electrochemical leaf. *Chem Rev* **123**, 5421-5458 (2023). https://doi.org:10.1021/acs.chemrev.2c00397

131 Megarity, C. F., Weald, T. R. I., Heath, R. S., Turner, N. J. & Armstrong, F. A. A nanoconfined four-enzyme cascade simultaneously driven by electrical and chemical energy, with built-in rapid, confocal recycling of NADP(H) and ATP. *ACS Catal* **12**, 8811-8821 (2022). https://doi.org:10.1021/acscatal.2c00999

132 Lee, Y. S., Lim, K. & Minteer, S. D. Cascaded biocatalysis and bioelectrocatalysis: overview and recent advances. *Annu Rev Phys Chem* **72**, 467-488 (2021). https://doi.org:10.1146/annurev-physchem-090519-050109
133 McMillan, D. G. G., Marritt, S. J., Butt, J. N. & Jeuken, L. J. C. Menaquinone-7 is specific cofactor in tetraheme quinol dehydrogenase CymA. *J Biol Chem* **287**, 14215-14225 (2012). https://doi.org:10.1074/jbc.M112.348813
134 Gutierrez-Sanchez, C. *et al.* Oriented immobilization of a membrane-bound hydrogenase onto an electrode for direct electron transfer. *Langmuir* **27**, 6449-6457 (2011). https://doi.org:10.1021/la200141t
135 Friedrich, M. G. *et al.* In situ monitoring of the catalytic activity of cytochrome *c* oxidase in a biomimetic architecture. *Biophys J* **95**, 1500-1510 (2008). https://doi.org:10.1529/biophysj.107.122747
136 Meyer, T. *et al.* Evidence for distinct electron transfer processes in terminal oxidases from different origin by means of protein film voltammetry. *J Am Chem Soc* **136**, 10854-10857 (2014). https://doi.org:10.1021/ja505126v
137 Holland, J. T., Lau, C., Brozik, S., Atanassov, P. & Banta, S. Engineering of glucose oxidase for direct electron transfer via site-specific gold nanoparticle conjugation. *J Am Chem Soc* **133**, 19262-19265 (2011). https://doi.org:10.1021/ja2071237
138 Adamson, H. *et al.* Analysis of HypD disulfide redox chemistry via optimization of Fourier Transformed ac voltammetric data. *Anal Chem* **89**, 1565-1573 (2017). https://doi.org:10.1021/acs.analchem.6b03589
139 Maiocco, S. J., Grove, T. L., Booker, S. J. & Elliott, S. J. Electrochemical resolution of the [4Fe-4S] centers of the AdoMet radical enzyme BtrN: evidence of proton coupling and an unusual, low-potential auxiliary cluster. *J Am Chem Soc* **137**, 8664-8667 (2015). https://doi.org:10.1021/jacs.5b03384
140 Jeuken, L. J. C., Jones, A. K., Chapman, S. K., Cecchini, G. & Armstrong, F. A. Electron-transfer mechanisms through biological redox chains in multicenter enzymes. *J Am Chem Soc* **124**, 5702-5713 (2002). https://doi.org:10.1021/ja012638w
141 Gulaboski, R. Theoretical contribution towards understanding specific behaviour of "simple" protein-film reactions in square-wave voltammetry. *Electroanal* **31**, 545-553 (2019). https://doi.org:10.1002/elan.201800739
142 Pilz, F. H. & Kielb, P. Cyclic voltammetry, square wave voltammetry or electrochemical impedance spectroscopy? Interrogating electrochemical approaches for the determination of electron transfer rates of immobilized redox proteins *BBA Advances 4* 100095 (2023). https://doi.org:10.1016/j.bbadva.2023.100095
143 Adamson, H., Bond, A. M. & Parkin, A. Probing biological redox chemistry with large amplitude Fourier transformed ac voltammetry. *Chem Commun* **53**, 9519-9533 (2017). https://doi.org:10.1039/c7cc03870d
144 Bell, C. G., Anastassiou, C. A., O'Hare, D., Parker, K. H. & Siggers, J. H. Theoretical treatment of high-frequency, large-amplitude ac voltammetry applied to ideal surface-confined redox systems. *Electrochim Acta* **64**, 71-80 (2012). https://doi.org:10.1016/j.electacta.2011.12.088

**HIGHLIGHTED REFERENCES:**


Leger, C. & Bertrand, P. Direct electrochemistry of redox enzymes as a tool for mechanistic studies. *Chem Rev* 108, 2379-2438 (2008). https://doi.org:10.1021/cr0680742

**This comprehensive review summarises several models developed to interpret the PFE of adsorbed redox proteins and enzymes, it also explains how the models are used to analyse experimental data**.

Colburn, A. W., Levey, K. J., O'Hare, D. & Macpherson, J. V. Lifting the lid on the potentiostat: a beginner's guide to understanding electrochemical circuitry and practical operation. *Phys Chem Chem Phys* 23, 8100-8117 (2021). https://doi.org:10.1039/d1cp00661d

**An excellent tutorial review on the operation of potentiostats and problem-solving issues that can arise with electrochemical measurements.**

Hirst, J. & Armstrong, F. A. Fast-scan cyclic voltammetry of protein films on pyrolytic graphite edge electrodes: Characteristics of electron exchange. *Anal Chem* 70, 5062-5071 (1998). https://doi.org:10.1021/ac980557l

**Rates of interfacial electron transfer are quantified for four different proteins, the resulting models consider Marcus and Butler-Volmer descriptions of interfacial electron transfer and form the foundations for many subsequent models of more complex behaviours.**

Baffert, C. *et al.* Covalent attachment of FeFe hydrogenases to carbon electrodes for direct electron transfer. *Anal Chem* 84, 7999-8005 (2012). https://doi.org:10.1021/ac301812s

**An excellent introduction to the benefits and complexities of covalent attachment of enzymes to electrodes for PFE.**

Mersch, D. *et al.* Wiring of Photosystem II to hydrogenase for photoelectrochemical water splitting. *J Am Chem Soc* 137, 8541-8549 (2015). https://doi.org:10.1021/jacs.5b03737

**This paper describes PFE using hierarchical inverse-opal ITO working electrodes prepared by a method now used by many different research groups.**

Kornienko, N. *et al.* Oxygenic photoreactivity in Photosystem II studied by rotating ring disk electrochemistry. *J Am Chem Soc* 140, 17923-17931 (2018). https://doi.org:10.1021/jacs.8b08784

**An elegant example of the power of PFE to deconvolute complexity in enzyme mechanism that benefits from the use of a rotating ring disk electrode.**

Laviron, E. General expression of the linear potential sweep voltammogram in the case of diffusionless electrochemical systems. *J Electroanal Chem* 101, 19-28 (1979). https://doi.org:10.1016/S0022-0728(79)80075-3

**This landmark paper derives equations for the non-catalytic voltammetry of adsorbed redox centres and that are used ubiquitously in the analysis of PFE.**

Butt, J. N. *et al.* Voltammetric characterization of rapid and reversible binding of an exogenous thiolate ligand at a [4Fe-4S] cluster in Ferredoxin III from *Desulfovibrio africanus*. *J Am Chem Soc* 115, 1413-1421 (1993). https://doi.org:10.1021/ja00057a026

**A comprehensive illustration of how PFE can detect and quantify chemical reactions coupled to redox transitions (EC and CE reactions).**

Hirst, J., Jameson, G. N. L., Allen, J. W. A. & Armstrong, F. A. Very rapid, cooperative two-electron/two-proton redox reactions of [3Fe-4S] clusters: Detection and analysis by protein-film voltammetry. *J Am Chem Soc* 120, 11994-11999 (1998). https://doi.org:10.1021/ja981693a

**An elegant account of the use of PFE to quantify the rates of redox-coupled proton (un)binding events.**

Milton, R. D. & Minteer, S. D. Direct enzymatic bioelectrocatalysis: differentiating between myth and reality. *J R Soc Interface* 14, 20170253 (2017). https://doi.org:10.1098/rsif.2017.0253

**Some important control studies that need to be done to ensure PFE responses are not due to artefacts such as dissociated co-factors are highlighed in the final section of this review article.**

Ash, P. A., Kendall-Price, S. E. T. & Vincent, K. A. Unifying activity, structure, and spectroscopy of [NiFe] hydrogenases: combining techniques to clarify mechanistic understanding. *Acc Chem Res* 52, 3120-3131 (2019). https://doi.org:10.1021/acs.accounts.9b00293

**An excellent review on the benefits of combining spectroscopy with PFE.**

Chen, X. L. *et al.* 3D-printed hierarchical pillar array electrodes for high-performance semi-artificial photosynthesis. *Nat Mater* 21, 811-818 (2022). https://doi.org:10.1038/s41563-022-01205-5

**Further progress in PFE will in part depend on improved electrode materials and this paper describes an elegant printing technique to create (nano)structured electrodes.**

Liu, Y. P. *et al.* Facile functionalization of carbon electrodes for efficient electroenzymatic hydrogen production. *JACS Au* 3, 124-130 (2023). https://doi.org:10.1021/jacsau.2c00551

**Application of PFE in catalysis requires high current densities and this paper describes a relatively easy way to achieve this with hydrogenases.**

**Glossary**

Chronoamperometry a technique in which electric current is measured as a function of time with the WE held at a defined electric potential, or stepped between two or more defined electric potentials.

Counter electrode – an electrode that carries electric current flowing in a three-electrode electrochemical cell. Electrochemical processes occurring at this electrode are not of interest.

Cyclic voltammetry – a technique in which the current is measured as the WE potential is ramped linearly with time. When a defined WE potential is reached, the potential is ramped linearly in the opposite direction to return the WE to its initial potential.

Faradaic current – electric current generated by the oxidation or reduction of species at a WE.

Non-Faradaic current – electric current measured in an electrochemical cell that is not due to redox processes. Typically, this current arises from migration of ions in response to the electric potential applied to an electrode.

Redox catalysis - the interconversion of reactants and products through a redox reaction catalysed by an enzyme. For an enzyme catalysed reaction the reactants are often referred to as substrates.

Reference electrode – an electrode with a stable and defined electrode potential. The potential of the working electrode is defined relative to that of the reference electrode.

Working electrode – the electrode at which redox chemistry of interest occurs in a three-electrode electrochemical cell.